



CAA PAPER 99002

**THE PROVISION OF GUIDELINES
FOR THE INSTALLATION
OF WIND TURBINES NEAR
AERONAUTICAL RADIO STATIONS**

CIVIL AVIATION AUTHORITY, LONDON, PRICE £7.50

CAA PAPER 99002

**THE PROVISION OF GUIDELINES
FOR THE INSTALLATION
OF WIND TURBINES NEAR
AERONAUTICAL RADIO STATIONS**

H S Dabis
R J Chignell

CIVIL AVIATION AUTHORITY, LONDON, APRIL 1999

© Civil Aviation Authority 1999

ISBN 0 86039 753 X

Printed and distributed by
Westward Digital Limited, 37 Windsor Street, Cheltenham, England

Executive Summary

This report describes work undertaken to establish guidelines for the safeguarding of aeronautical radio systems in the vicinity of wind farms. It covers three main tasks: the validation of previously developed theoretical models for the prediction of the wind turbine's radar cross section, the development of terrain models to take into account a number of obstacles in the radio paths and the development of software to assist in the assessment of the suitability of the establishment of a wind farm near a radio system or vice versa.

Wind turbines affect electromagnetic signals incident upon them causing multipath interference effects. The level of interference can cause incorrect information to be received. Additionally, the blades' rotation modulates the signals and this modulation may degrade the performance of aeronautical radio systems.

In order to quantify these interference effects, the characteristics of wind turbines need to be known. An important parameter is the radar cross section (RCS). Previous work at Emrad has concentrated specifically on investigating the various techniques for predicting the RCS of complex targets. Of the techniques investigated Physical Optics is considered to be the most effective in terms of accuracy of the results and computational efficiency. A theoretical model has been developed for predicting the RCS and the modulation effects due to the rotation of the blades. The model corresponds well to previously published results and with initial experimental measurements.

However, to enable the model to be used in practice, further validation was required. Measurements needed to be carried out in a well controlled environment where all effects apart from those generated by the turbine could be eliminated. These validation experiments were carried out at an antenna range, a site normally used for calibrating antenna characteristics where reflections from the ground and from other targets at the site are minimised. The tests were performed using a 20:1 scale model turbine mounted on a specially designed platform, which enabled the turbine response to be measured easily at various incident and observation angles. The test results agree well with those predicted by the model.

Also considered in this report are terrain effects. Although the RCS predictions are an important part in the computation of the interference levels at the receiver, obstacles in the radio path can also have a substantial effect. This report describes a model developed which takes into account a maximum of two terrain obstacles between the transmitter, wind turbine and receiver paths. There is good agreement with previously published results.

Software, which can run on any PC based system, has been written and tested in C++. This software enables the user to input the various parameters of the radio system under consideration. Based on these parameters, the programme computes the level of interference at the receiver, which can be compared with the allowable maximum value. Further investigation may then be undertaken if appropriate.

Contents

	<i>Page</i>
GLOSSARY	viii
1 INTRODUCTION	1
2 THEORETICAL MODEL VALIDATION TESTS	2
2.1 Antenna Range Description	3
2.2 Compact Range Measurements	6
2.3 Receiver Platform and Equipment	6
2.4 Sources of Measurement Inaccuracies	10
2.5 Measurements and Model Comparisons	12
2.5.1 RCS Measurements	12
2.5.1.1 Comparisons with theoretical models for a metallic plate	12
2.5.1.2 Comparisons with theoretical models for scale model turbine	16
2.5.1.3 Remarks on Comparison Results	28
2.5.2 Modulation Measurements	28
2.5.2.1 Remarks on Modulation Results	43
3 TERRAIN MODELLING	44
3.1 Model Development and Comparison Results	44
4 GUIDELINE FORMULATION	45
4.1 Parameter Definition	45
4.2 Theoretical Formulation	46
4.2.1 Indirect Path Signal Calculation	46
4.2.2 Direct Path Signal Calculation	46
4.2.3 Carrier to Interference Ratio Calculation	46
5 SOFTWARE IMPLEMENTATIONS	46
5.1 Terrain Model Programme	47
5.2 Radar Cross Section Model Programme	47
5.3 Carrier To Interference Programme	47
6 CONCLUSIONS	48
7 REFERENCES	48
Appendix A TERRAIN MODEL THEORETICAL FORMULATION	49

LIST OF FIGURES

	<i>Page</i>
Figure 1(a) A schematic of antenna range	4
Figure 1(b) A photograph of the antenna range used for measurements	5
Figure 2(a) Wind Turbine test platform	7
Figure 2(b) A photograph of test set-up	8
Figure 3(a) A block diagram of measurement equipment	9
Figure 3(b) A photograph of control and measurement equipment	9
Figure 4 Diagram showing situations of measurement difficulty	
(a) Dish blocking transmit path	11
(b) Dish in line with transmit path	11
Figure 5 Incident and observation angles relative to the turbine blades	13
Figure 6 RCS comparisons between theoretical predictions (solid line) and measurements (dashed line) at different incident angles for a metallic plate.	
(a) Incident angle = 57°	14
(b) Incident angle = 62°	14
(c) Incident angle = 67°	15
Figure 7 RCS comparisons for scale model turbine at 5.5 GHz (Horizontal Polarisation)	
(a) Incident angle = 60°	17
(b) Incident angle = 50°	17
(c) Incident angle = 40°	18
Figure 8 RCS comparisons for scale model turbine at 5.5 GHz (Vertical Polarisation)	
(a) Incident angle = 60°	19
(b) Incident angle = 50°	19
(c) Incident angle = 40°	20
Figure 9 RCS comparisons for scale model turbine at 5.0 GHz (Vertical Polarisation)	
(a) Incident angle = 60°	21
(b) Incident angle = 50°	21
(c) Incident angle = 40°	22
Figure 10 RCS comparisons for scale model turbine at 5.0 GHz (Horizontal Polarisation)	
(a) Incident angle = 60°	23
(b) Incident angle = 50°	23
(c) Incident angle = 40°	24
Figure 11 RCS comparisons for scale model turbine at 3.2 GHz (Vertical Polarisation)	
(a) Incident angle = 60°	25
(b) Incident angle = 50°	25
(c) Incident angle = 40°	26

Figure 12	RCS comparisons for scale model turbine at 3.2 GHz (Horizontal Polarisation)	
	(a) Incident angle = 60°	27
	(b) Incident angle = 50°	27
	(c) Incident angle = 40°	28
Figure 13	Modulation Results. Incident angle = 60°, Observation = 100°, Horizontal Polarisation, 5.5 GHz	
	(a) Time waveform comparison	30
	(b) Spectrum comparison	30
	(c) Spectrum comparison	31
Figure 14	Modulation Results. Incident angle = 60°, Observation = 140°, Horizontal Polarisation, 5.5 GHz	
	(a) Time waveform comparison	32
	(b) Spectrum comparison	32
	(c) Spectrum comparison	33
Figure 15	Modulation Results. Incident angle = 60°, Observation = 150°, Horizontal Polarisation, 5.5 GHz	
	(a) Time waveform comparison	34
	(b) Spectrum comparison	34
	(c) Spectrum comparison	35
Figure 16	Modulation Results. Incident angle = 60°, Observation = 100°, Horizontal Polarisation, 5.0 GHz	
	(a) Time waveform comparison	36
	(b) Spectrum comparison	36
	(c) Spectrum comparison	37
Figure 17	Modulation Results. Incident angle = 60°, Observation = 140°, Horizontal Polarisation, 5.0 GHz	
	(a) Time waveform comparison	38
	(b) Spectrum comparison	38
	(c) Spectrum comparison	39
Figure 18	Modulation Results. Incident angle = 60°, Observation = 100°, Vertical Polarisation, 3.2 GHz	
	(a) Time waveform comparison	40
	(b) Spectrum comparison	40
	(c) Spectrum comparison	41
Figure 19	Modulation Results. Incident angle = 60°, Observation = 140°, Vertical Polarisation, 3.2 GHz	
	(a) Time waveform comparison	42
	(b) Spectrum comparison	42
	(c) Spectrum comparison	43

LIST OF TABLES

		<i>Page</i>
Table 2.1	Modulation index for various parameters (Incident angle 60°)	29
Table 3.1	Comparison of diffraction loss using different techniques	44

GLOSSARY

BCD	Binary Coded Digit
CAA	Civil Aviation Authority
C/I	Carrier to Interference Ratio
EMI	Electromagnetic Interference
ILS	Instrument Landing System
LOS	Line of Sight
PC	Personal Computer
PO	Physical Optics
RCS	Radar Cross Section

INTRODUCTION

Despite the many advantages wind energy provides, there are some problems associated with wind farm installations. One of these is Electromagnetic Interference (EMI), caused by multipath effects generated by wind turbines which superimpose themselves upon the direct path signals. Additionally, the wind turbines' blade rotation causes modulation effects, which need to be considered.

Electromagnetic effects caused by wind turbines are not well understood. When an electromagnetic signal is incident upon a target some of the energy is absorbed and the rest is reflected. The amount of reflected signal depends on the wind turbine's size, shape, and location. The common term used for this is the radar cross section (RCS) of the target. With a knowledge of the maximum RCS value of the wind turbine, its effects on a nearby radio system can then be predicted. To make a decision upon the suitability of the installation of a wind farm before it has been built there is a need to be able to predict the wind turbines' RCS theoretically.

Previous work at Emrad [1] concentrated on developing a model to predict the RCS of wind turbines. The model is based on Physical Optics (PO) which has been proven to work well when the targets' size is large compared to the wavelength of the incident signal. In addition to giving accurate results, PO has the advantage of being a computationally efficient technique for calculating the RCS. The model can also be used to predict the modulation effects due to the blade rotation.

The experimental validation of the model forms an important part of the development process. During the initial stages of development of the model some validation was undertaken. However, it was considered necessary to perform a further set of tests before full confidence could be established in the model. To obtain accurate measurements, a controlled environment, which eliminates all unnecessary sources of error (mainly reflections), is required. There are essentially two possible solutions: an anechoic chamber or an antenna range.

Anechoic chambers provide an excellent environment for performing the controlled experiments, however, the size requirements for performing bistatic measurements in the far field and the frequency range of interest for this project made this an impractical option.

An antenna range is a large site normally used for characterising various types of antennas. It is essentially a large field of a few hundred metres length and width consisting of a number of transmit and receive locations each covering a certain frequency range. In normal usage an antenna is mounted at the receive end and its output is measured at various incident angles producing the antenna pattern. The validation tests performed for this project required bistatic measurements to be conducted in the far field region. The term bistatic describes a system where the transmitter and receiver are not co-located. The far field region is dependent upon the frequency of the signal and the size of target. For our set of tests a 20:1 scale model turbine and frequencies in the range of 3-6 GHz, the transmitter and receiver would need to be at least twenty one metres from the wind turbine. As it is impractical for the receiver to be moved in such a large radius around the turbine, a technique known as compact range measurements was used.

The basic principle of this technique is to simulate the far field situation at much reduced distances through the use of an offset parabolic reflector. The reflector converts the spherical waves incident upon it into plane waves which can be received using a horn feed. The experiments carried out in the antenna range used a fixed location for the transmitter and a compact range set-up as the receiver. This enabled the turbine characteristics to be measured easily at many different observation angles.

The other major part of the work concentrated upon the development of terrain models to take into account the effects of obstructions on the attenuation of the signals. Previous work assumed a flat earth model and therefore only took into account attenuation in the signal due to free space losses and the wind turbine reflections. The terrain effects can be either advantageous or disadvantageous depending on obstacle positions in the radio path. The developed model can take into account a maximum of two obstacles and is based on the work of Vogler [4]. Comparisons with other results [2,3] where actual field data was measured are favourable.

The guidelines involve computing the carrier to interference ratio (C/I) at the receiver for a particular radio system. By comparing these values with the minimum acceptable, the effect of the wind turbine on the radio system can be determined. It should be noted that different radio systems have different requirements depending on the minimum receiver threshold and the geometry of the system. A description of the minimum specifications for aeronautical system can be found in [5].

Finally a software suite has been written in C++ running in a PC environment. It computes the C/I ratio at the receiver. The software first calculates the various attenuations due to terrain in the radio paths. It then computes the RCS of the wind turbine and consequently the C/I at the receiver which is compared with the minimum required. The final result gives a simple and clear indication whether the effect of the turbines is serious enough to warrant further investigation.

2 THEORETICAL MODEL VALIDATION TESTS

This chapter describes the test procedures and set-up used for performing the RCS and modulation measurements on a 20:1 scale wind turbine model. The measurements were used to validate the theoretical models. It describes the antenna range, the equipment used and compares the test results with the theoretical model solutions.

In order to fully validate the theoretical model the system parameters were used as follows:

- Three frequencies (3.2 GHz, 5.0 GHz and 5.5 GHz). Note that since the measurements were carried out on a 20:1 scaled down model wind turbine, these frequencies are equivalent to 160MHz-275MHz tests on a real size turbine.
- Three incident angles (30°, 40° and 50°).
- Observation angles in steps of 0.5° around the turbine for each incident angle.

- Vertical and Horizontal Polarisation.

All of the measurement data were transferred to a PC and stored digitally.

2.1 **Antenna Range description**

Antenna ranges are normally used for performing accurate antenna pattern measurements. The equipment used on a range is calibrated with reflections of spurious targets and ground reflections minimised. The site consists of different ranges, each associated with a different frequency band.

Figure 1(a) shows an overall schematic of the antenna range used for carrying out the tests. Figure 1(b) is a photo of the range used. It is owned by DERA and situated at Funtington. The overall site dimensions are 500mx500m. Figure 2 shows a more detailed diagram of the set-up used for the test measurements.

The transmitter position was kept constant throughout the tests. The receiver and the scale model turbine could, however, be rotated independently about their vertical axis. Hence the incident and observation angles could be easily varied.

A frequency synthesiser was used to transmit the required frequency. Both frequency and output power were easily adjusted by varying the synthesiser parameters. The transmit feed was rotated to generate vertical or horizontal polarisation.

The turbine was mounted on a rotating upper azimuth receive tower while the dish supporting platform was mounted on a different rotating lower azimuth platform. Both of these platforms could be rotated independently enabling full control of the incident and observation angles. The tower was approximately 15 m high.

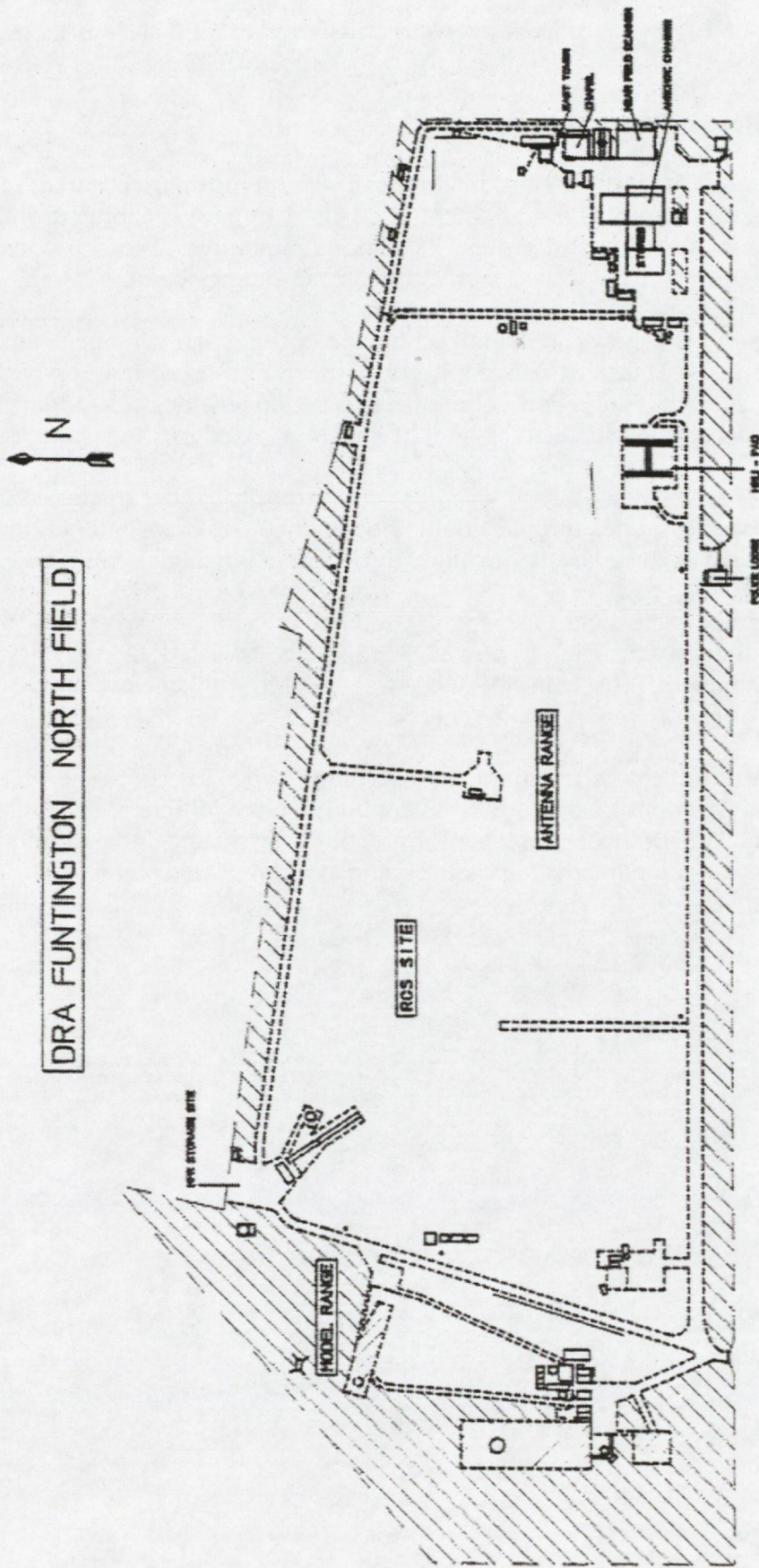


Figure 1(a) A schematic of antenna range



Figure 1(b) A photograph of the antenna range used for measurements

2.2 Compact Range Measurements

The developed theoretical model for predicting the radar cross section of a target assumes that the transmitter and receiver are in the far field regions where the travelling waves are assumed planar and not spherical. This distance is defined as $2D^2/\lambda$, where $D(m)$ is the target's largest dimension and $\lambda(m)$ is the wavelength. In practice this can be relaxed to half the distance without introducing any noticeable errors. For the tests to be conducted in the far field the transmitter and receiver would need to be at least 21m away from the turbine. Although these distances are not exceedingly large for the antenna range, performing the bistatic measurements at different observation angles would be impractical.

Therefore, an alternative method was used. The receiver was placed close to the target and an offset parabolic dish was used to convert the spherical waves into plane waves simulating the far field region. This is known as the compact antenna range set-up. A diagram of this is shown in Figure 2(a) where the receiver dish is placed at the end of a mechanical platform approximately 2m from the turbine. The platform can then be rotated around the turbine and accurate measurements of the observation angles can be taken. Figure 2(b) is a photo of the compact range set-up.

2.3 Receiver Platform and Equipment

A 1.8m offset parabolic reflector was used to receive the signals reflected off the wind turbine. It was mounted on a platform 2m away from the turbine with a horn feed at the focus point of the dish. Two different feeds were used to allow for a wider range of frequency measurements.

The output of the feed (i.e. the received signal) was then fed via an RF cable to a control tower where all the measurements could be made. Figure 3(a) is a schematic of the measurement equipment used. Figure 3(b) is a photo of the actual equipment used.

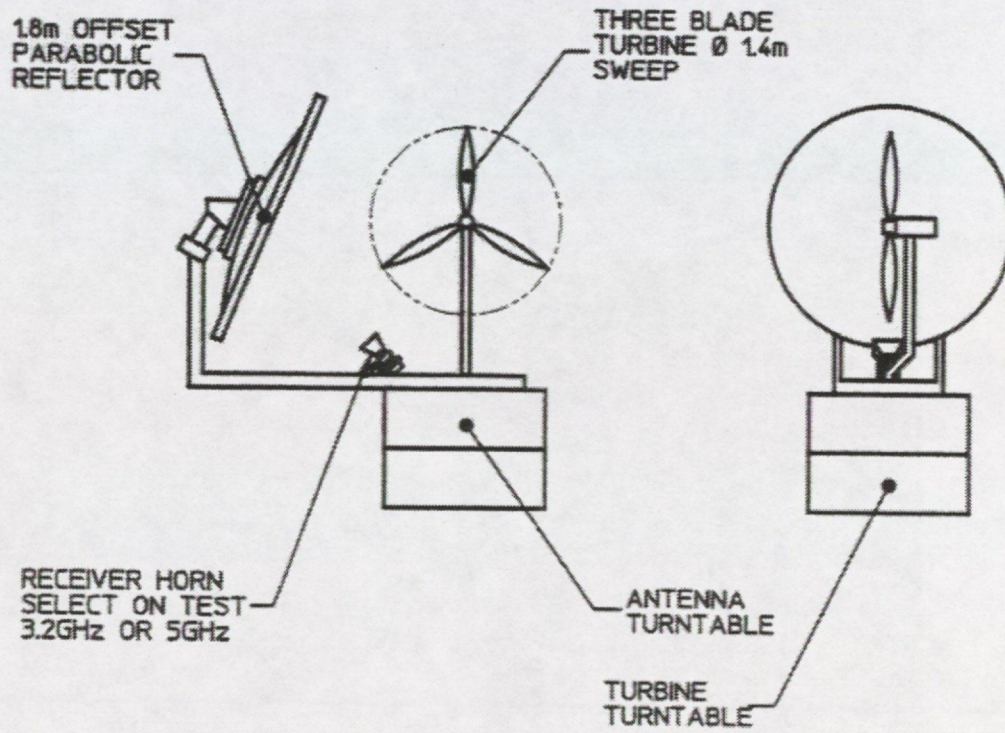
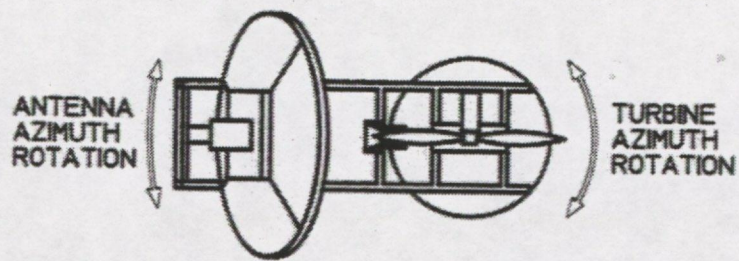


Figure 2(a) Wind Turbine test platform

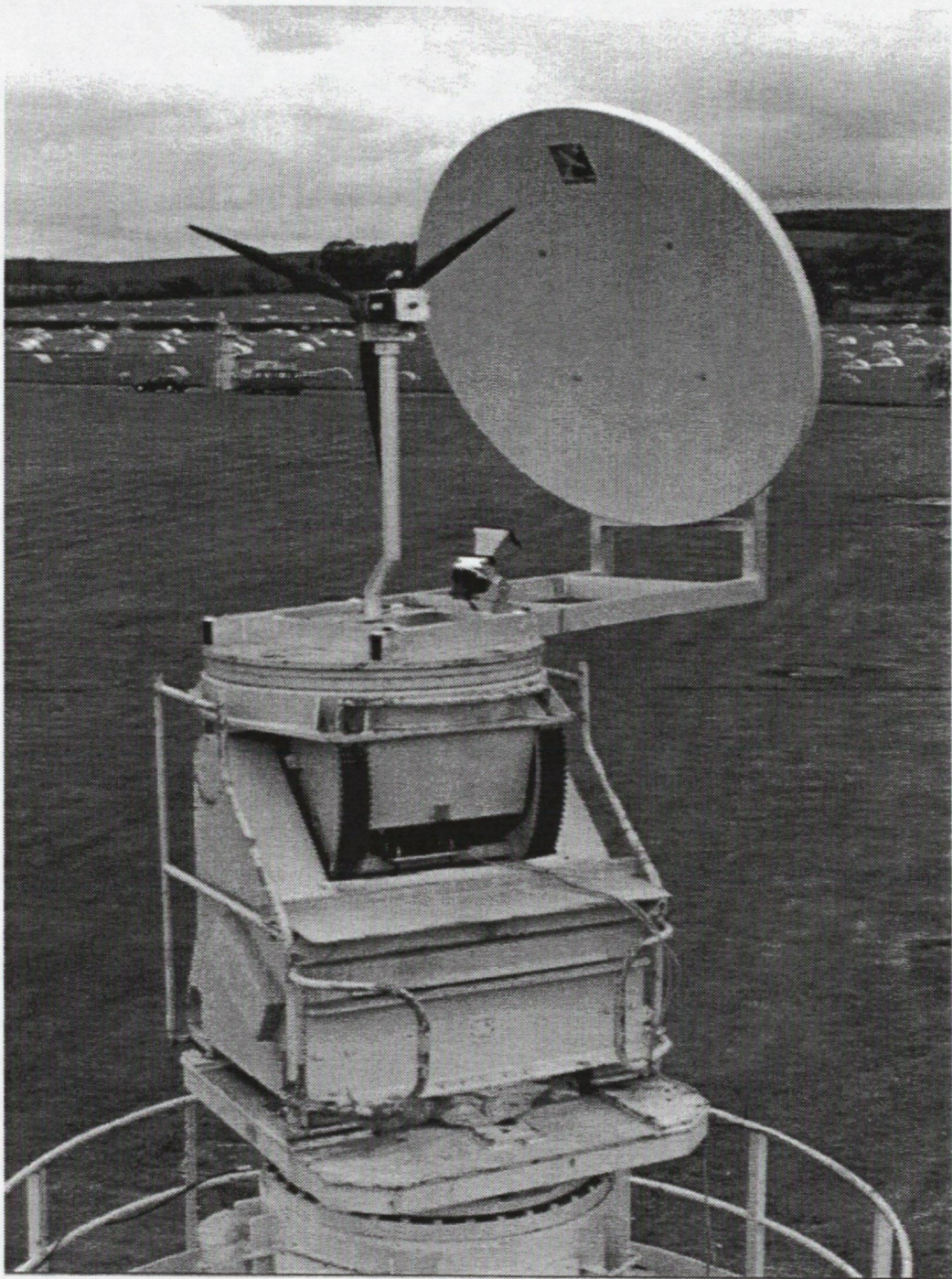


Figure 2(b) A photograph of test set-up

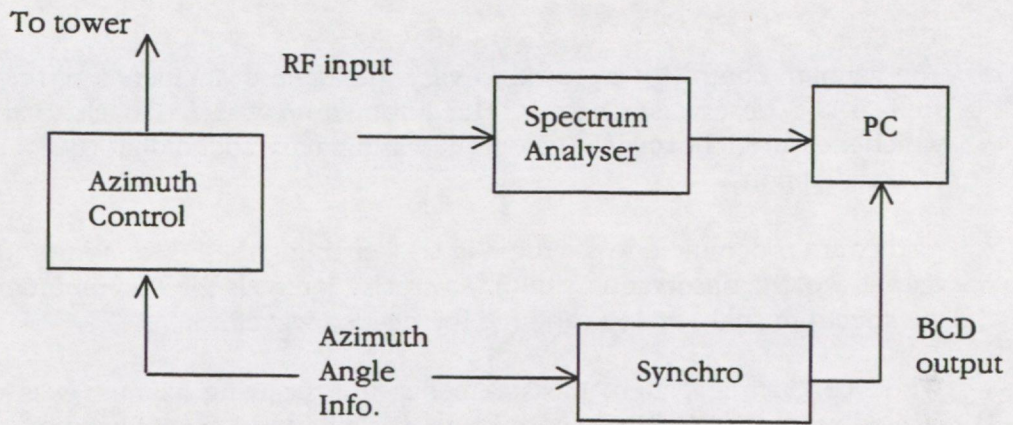


Figure 3(a) A block diagram of measurement equipment

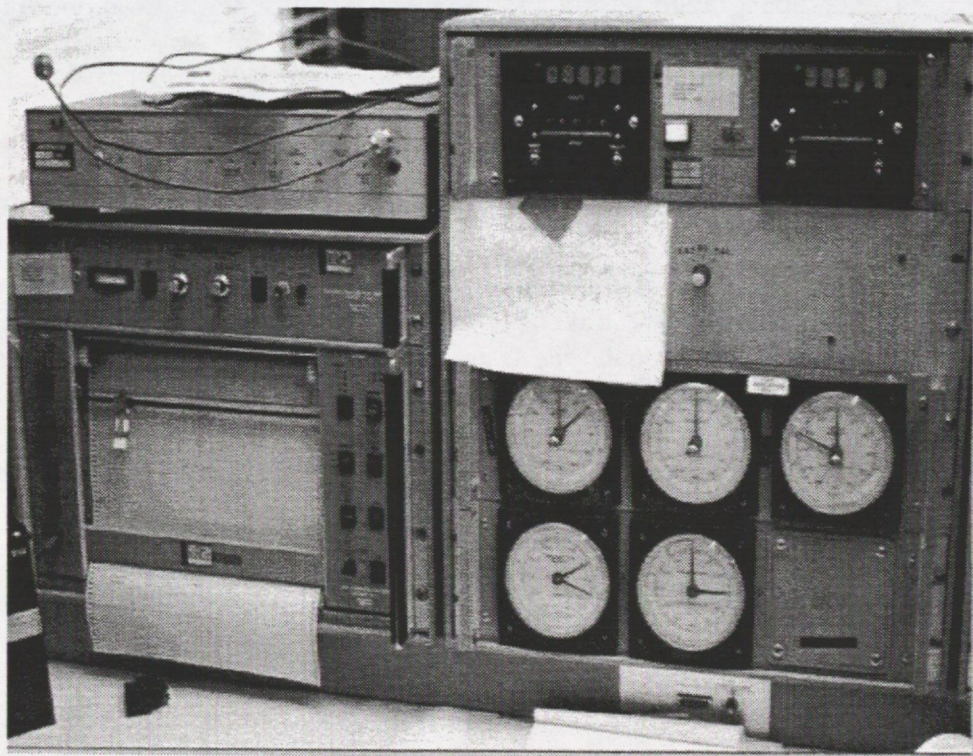


Figure 3(b) A photograph of control and measurement equipment

The azimuth controls were used to vary the angle of incidence of the turbine as well as the observation angles. The information was fed back to the synchro which measured the angle. The output was a binary coded digit (BCD) code to the PC parallel port.

A software programme was written in C++ enabling the PC to monitor the synchro output (i.e. the observation angle). At precise intervals the PC communicated with the spectrum analyser and captured the desired waveform.

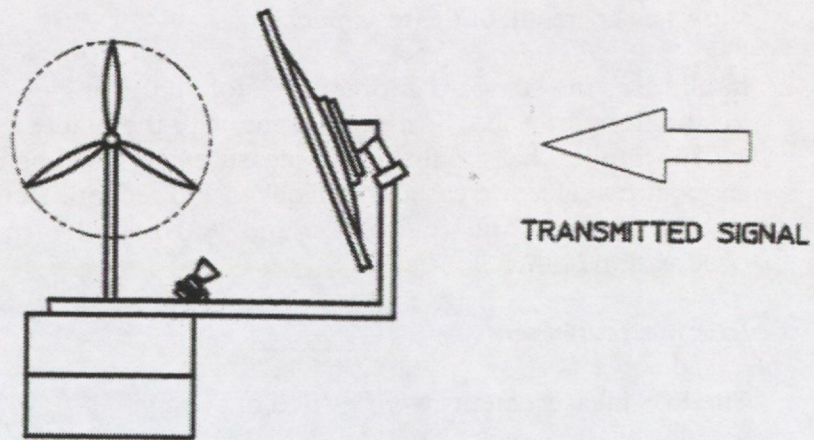
When conducting pattern measurements, the receiving azimuth was continually rotated using the PC. When modulation was measured, manual control was used.

A spectrum analyser was used to receive and display the signal. Two different settings were used. Firstly, a frequency span of 10 MHz around the centre frequency was used to capture the antenna patterns (with and without the turbine). Secondly, a zero span (at the centre frequency) with a 3 second duration was used to measure the modulation effects. Using an interface card, the PC had full access to all the data. This enabled full digital storage of all the measurements carried out.

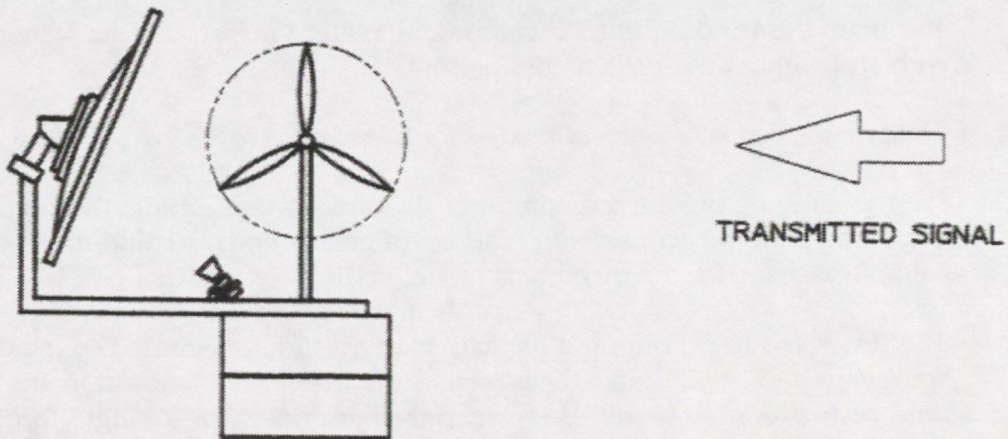
2.4 Sources of Measurement Inaccuracies

The compact range set-up, and the mechanical platform used, were both designed to reduce measurement inaccuracies to a minimum. Nevertheless, there were still unavoidable sources of inaccuracies which will now be discussed:

- *Dish in front of the turbine blocking the transmitter path (Figure 4a):* A very small amount of signal will get around the dish and onto the turbine making it very difficult to detect any reflected signal.
- *Dish behind turbine facing transmitter (Figure 4b):* The received signal is dominated by the direct path signal of the transmitter. The dynamic range of the spectrum analyser is not wide enough for such small signals to be detected.
- *Inaccuracies of measuring equipment:* These could be attributed to errors in the calibration of the electronic equipment due to temperature variations.
- *Wind variations:* Variations in wind could have an effect on the amplitude of the received signal.



a) DISH BLOCKING TRANSMIT PATH



b) DISH IN LINE WITH TRANSMIT PATH

Figure 4 Diagram showing situations of measurement difficulty

2.5 **Measurements and Model Comparisons**

The full set of test measurements completed is presented in appendices B and C to this report (available upon request from the CAA). In this section the results will be compared with the theoretical model predictions and a sample is presented.

Two sets of measurements were carried out. The RCS and the modulation. Figure 5 shows a schematic of the tests performed.

In all cases the standard adopted was for all the angles (incident and observation) to start at point A in a horizontal plane with the blades vertical as shown in Figure 5. This implies that the first set of measurements will be blocked by the dish. In all cases, the angles increased in a clockwise direction. Hence the angle of incidence is that between the transmitter and A while the receiver is from A to the observation point.

2.5.1 **RCS measurements**

The RCS measurements were carried out using:

1. Three different frequencies 3.2 GHz, 5.0 GHz and 5.5 GHz.
2. Vertical and Horizontal Polarisation.
3. Three incident angles (40°, 50° and 60°).
4. Observation angles at intervals of 0.5°.

To obtain the wind turbine's response, the pattern measurements were carried out with and without the scale model present.

2.5.1.1 *Comparisons with theoretical models for a metallic plate*

Prior to carrying out the tests on the scale model wind turbine, the simpler case of a metallic plate was considered. This set of measurements could then be used as a calibration stage for the theoretical model verification process.

The test was carried out on a metallic plate (0.45m x 0.45m). The incident angles were varied (57°, 62° and 67°) as well as the full set of observation angles. Due to time restrictions, however, this was only performed for a single frequency (3.2 GHz) horizontally polarised. In Figure 6 the responses of the plate for different incident angles are shown.

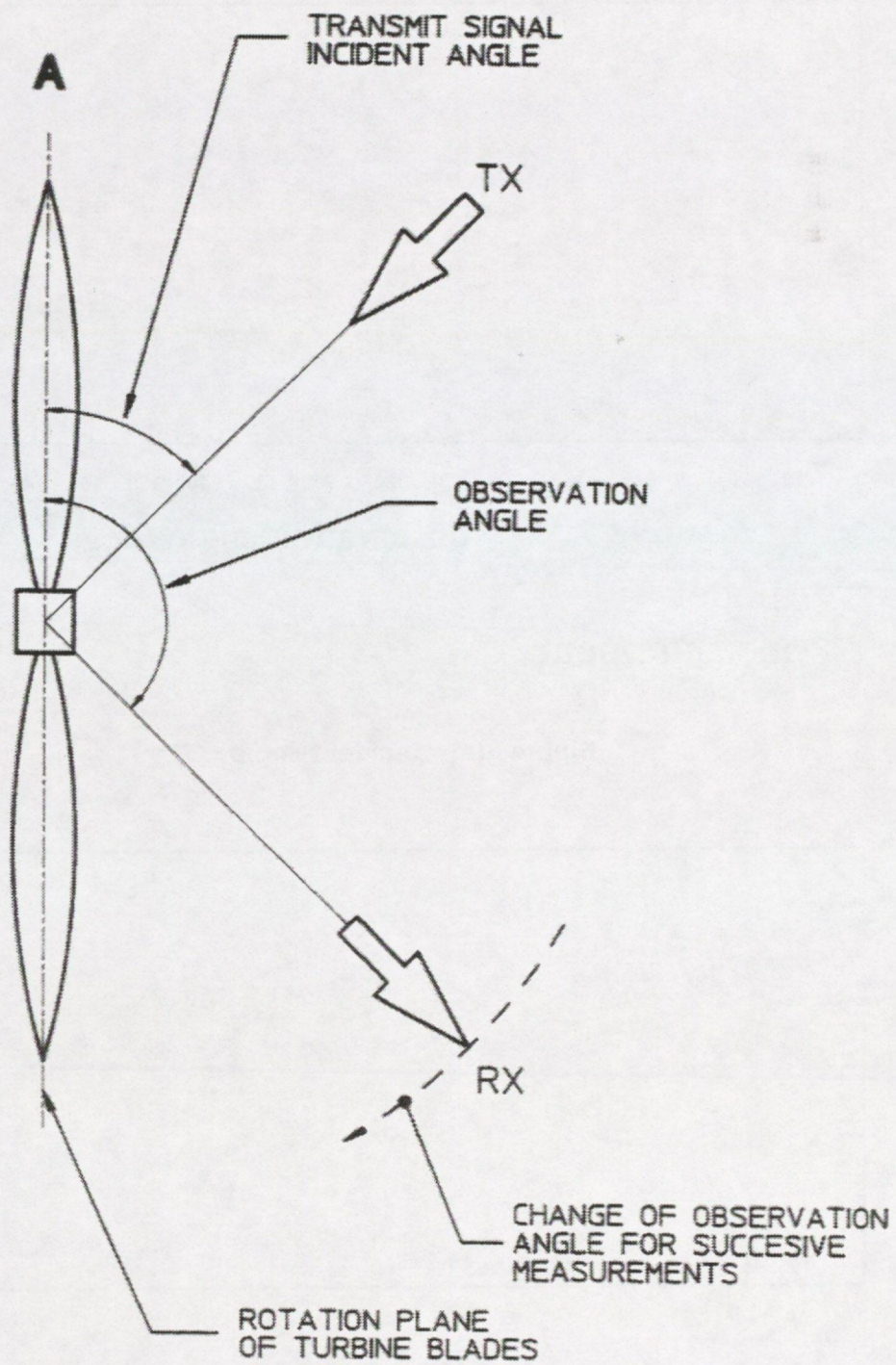


Figure 5 Incident and observation angles relative to the turbine blades

Figure 6 RCS comparisons between theoretical prediction (solid line) and measurements (dashed line) at different angles for a metallic plate

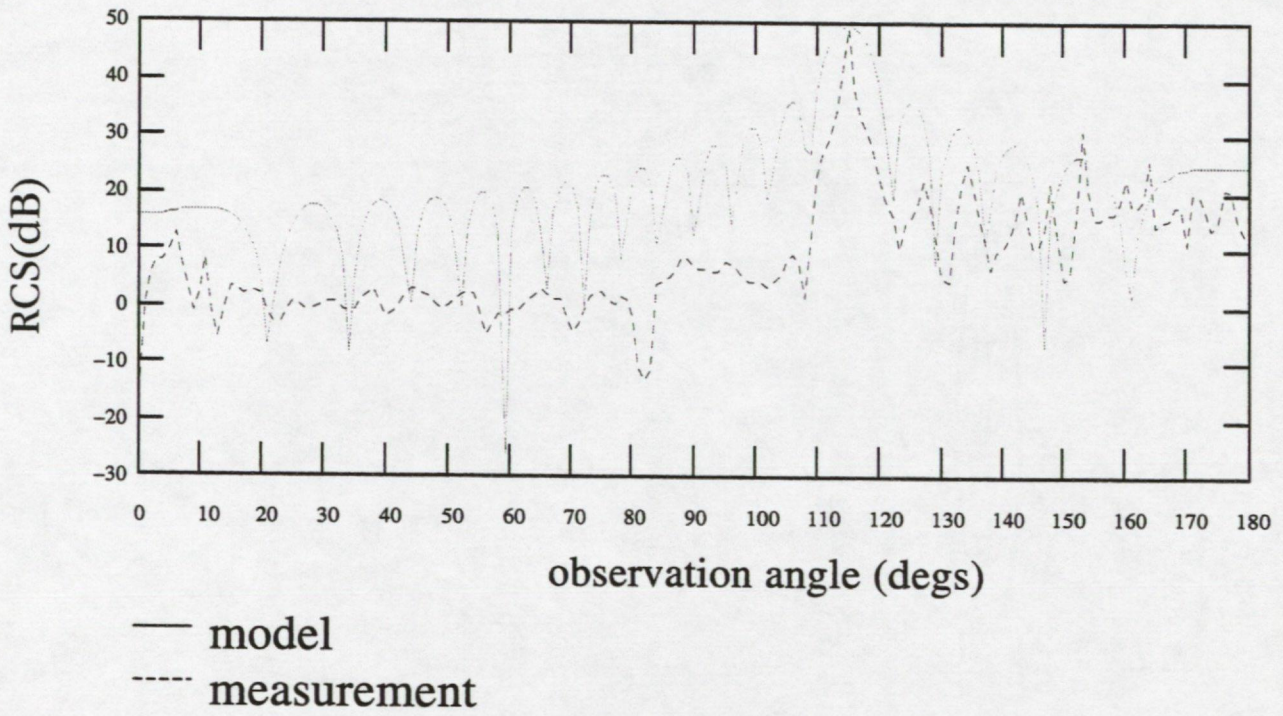


Figure 6(a) Incident angle = 57°

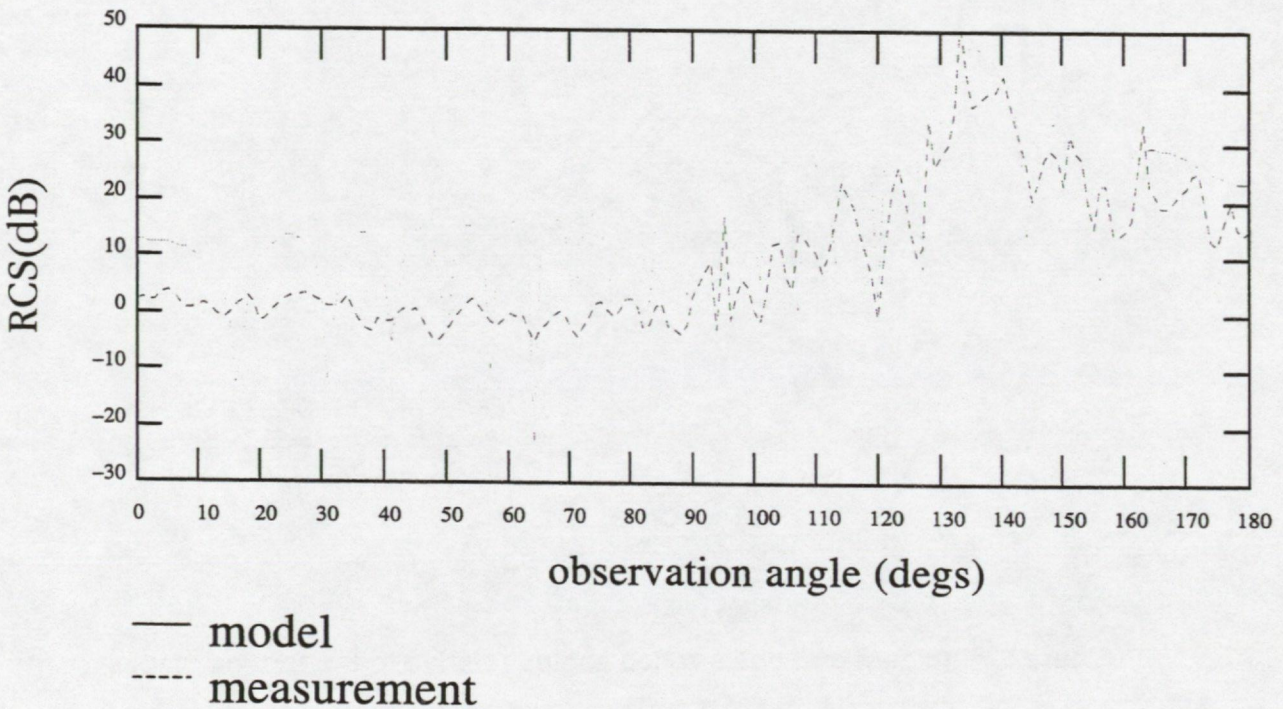


Figure 6(b) Incident angle = 62°

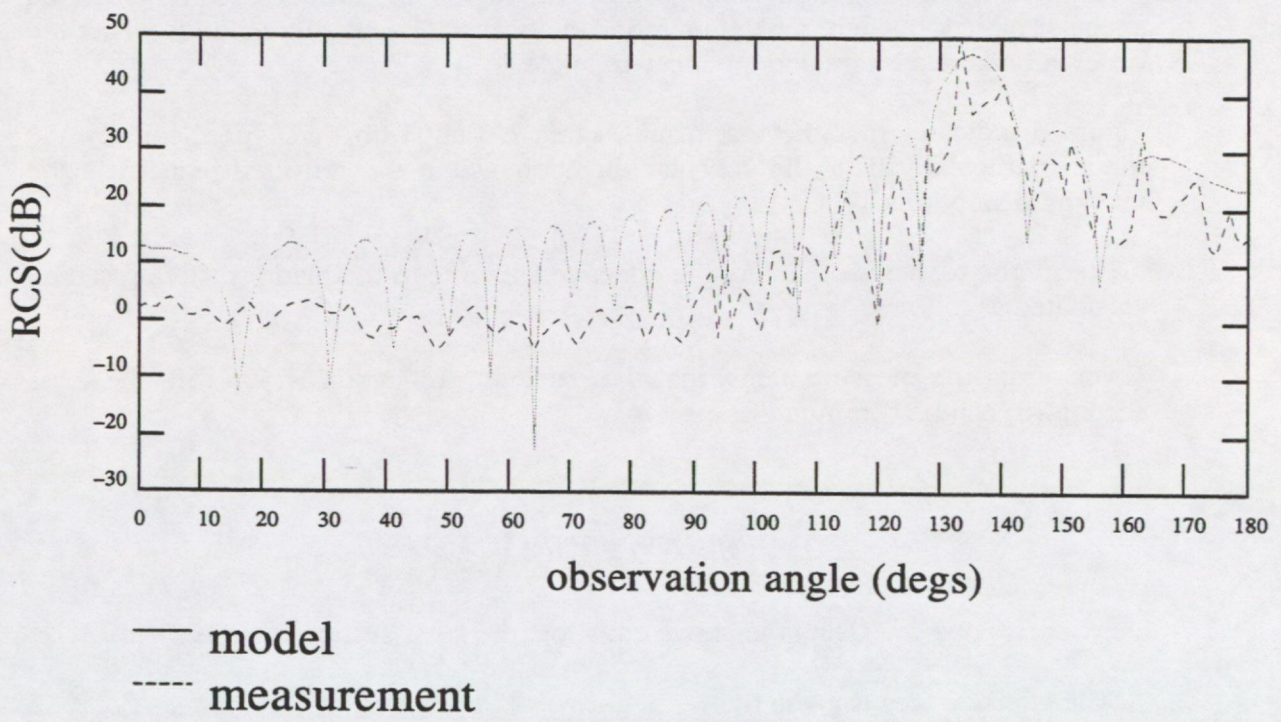


Figure 6(c) Incident angle = 67°

When performing the RCS comparisons, the region of most interest is near the specular direction where maximum reflection occurs. Specular direction is where the observation angle is equal to the incident angle.

Figure 6 indicates that the test results agree closely with those predicted by the model particularly near the specular direction where the reflected signal has the maximum amplitude.

To verify the readings obtained, the effective area due to the blade scattering can be calculated as follows:

Given, from the measurements, that the maximum reflection is 50.2 dB, the cross section (σ) can be computed from:

$$\text{Reflection} = 10 \log \left(\frac{4\pi\sigma}{\lambda^2} \right)$$

where $\lambda = 9.4$ cm. Using the above equation, the cross section $\sigma = 73.237$ m².

The effective area is given by:

$$\begin{aligned} A_e &= \lambda \sqrt{\frac{\sigma}{4\pi}} \\ &= 0.206 \text{ m}^2 \end{aligned}$$

which is in excellent agreement with the actual area of 0.226 m².

2.5.1.2 *Comparisons with theoretical models for scale model turbine*

As expected, the scale model turbine results were more complicated than those for the simple metallic rectangular plate considered earlier. However, the model still compares well with the test measurements particularly near the specular direction. Figures 7 – 12 show the results obtained.

**Figure 7 RCS comparisons for scale model turbine at 5.5 GHz
(Horizontal Polarisation)**

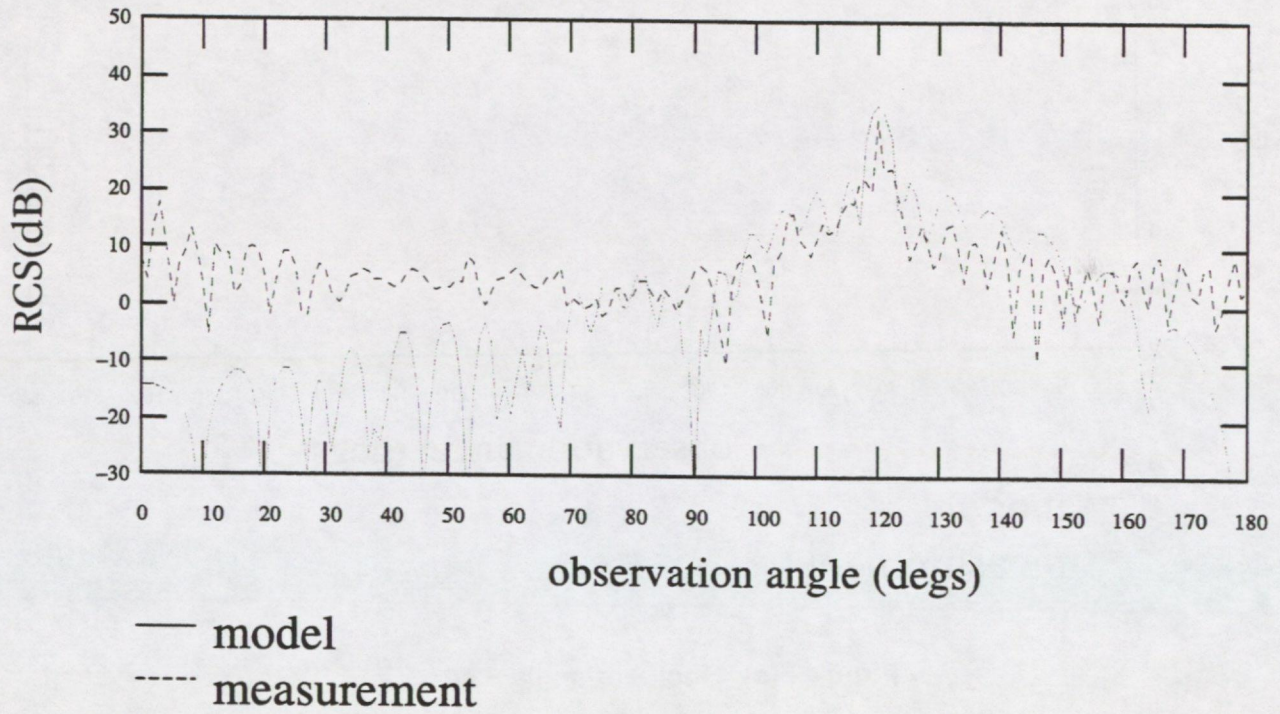


Figure 7(a) Incident angle = 60°

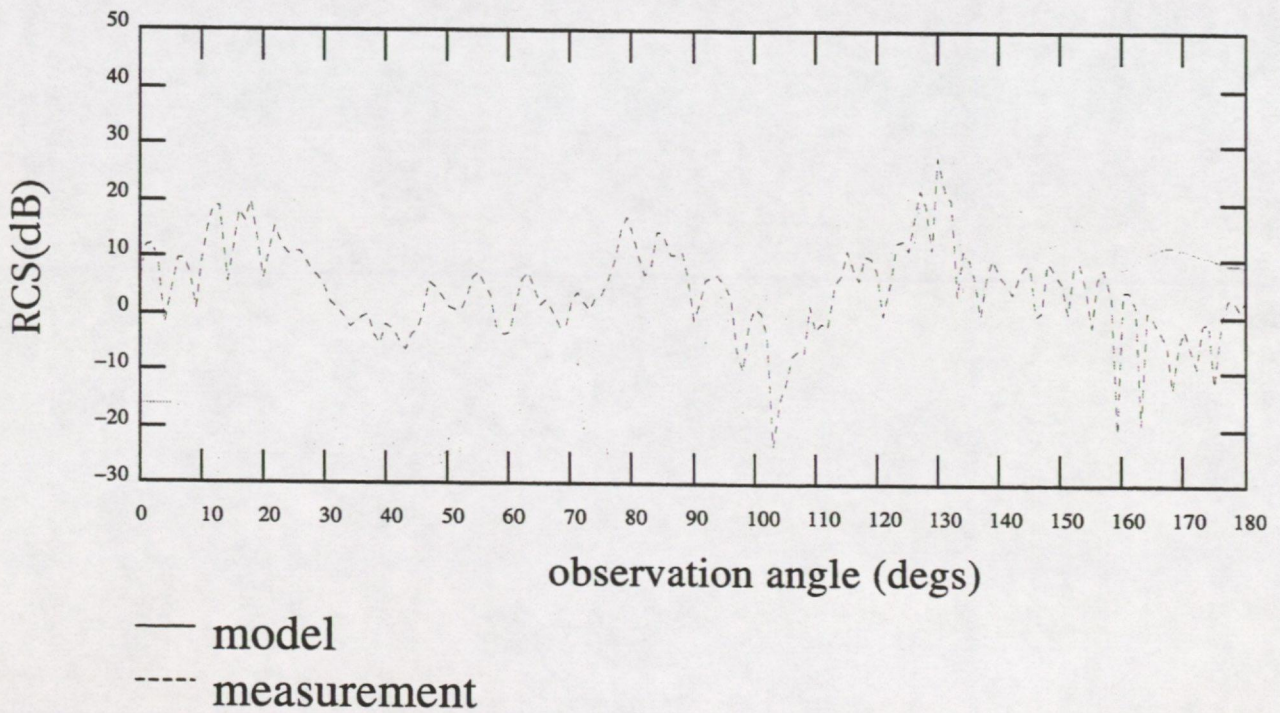


Figure 7(b) Incident angle = 50°

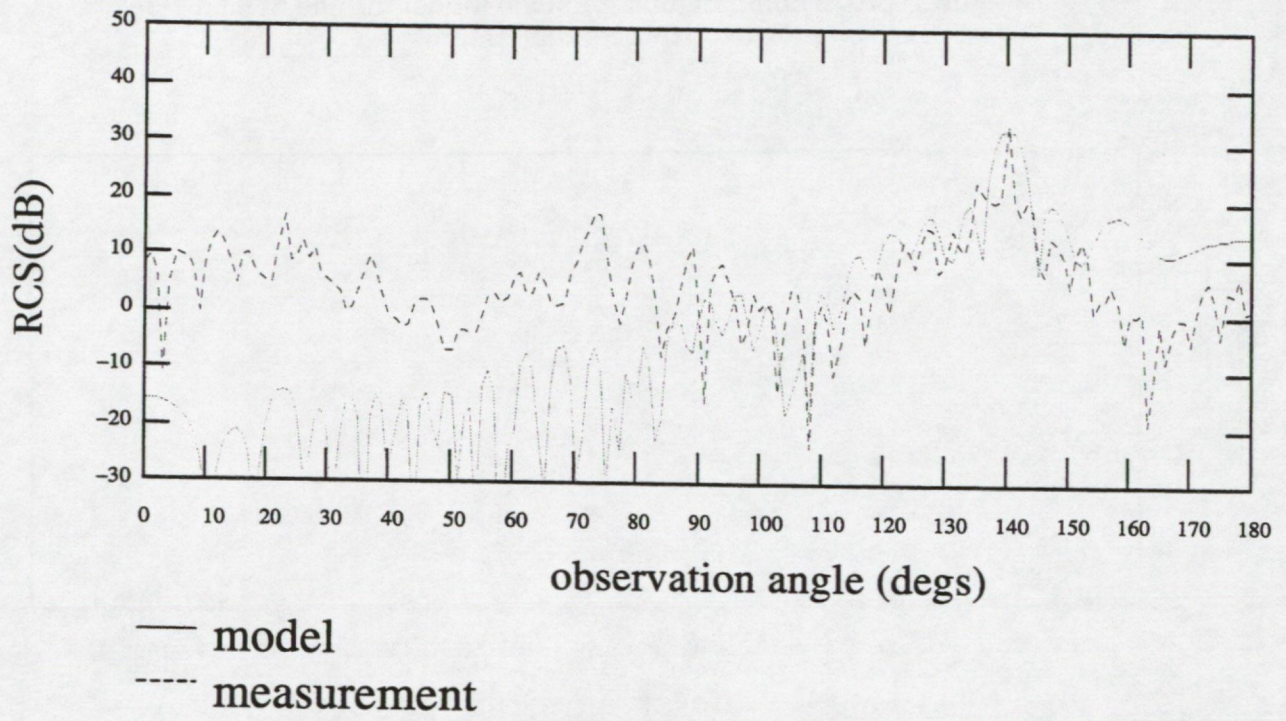


Figure 7(c) Incident angle = 40°

**Figure 8 RCS comparisons for scale model turbine at 5.5 GHz
(Vertical Polarisation)**

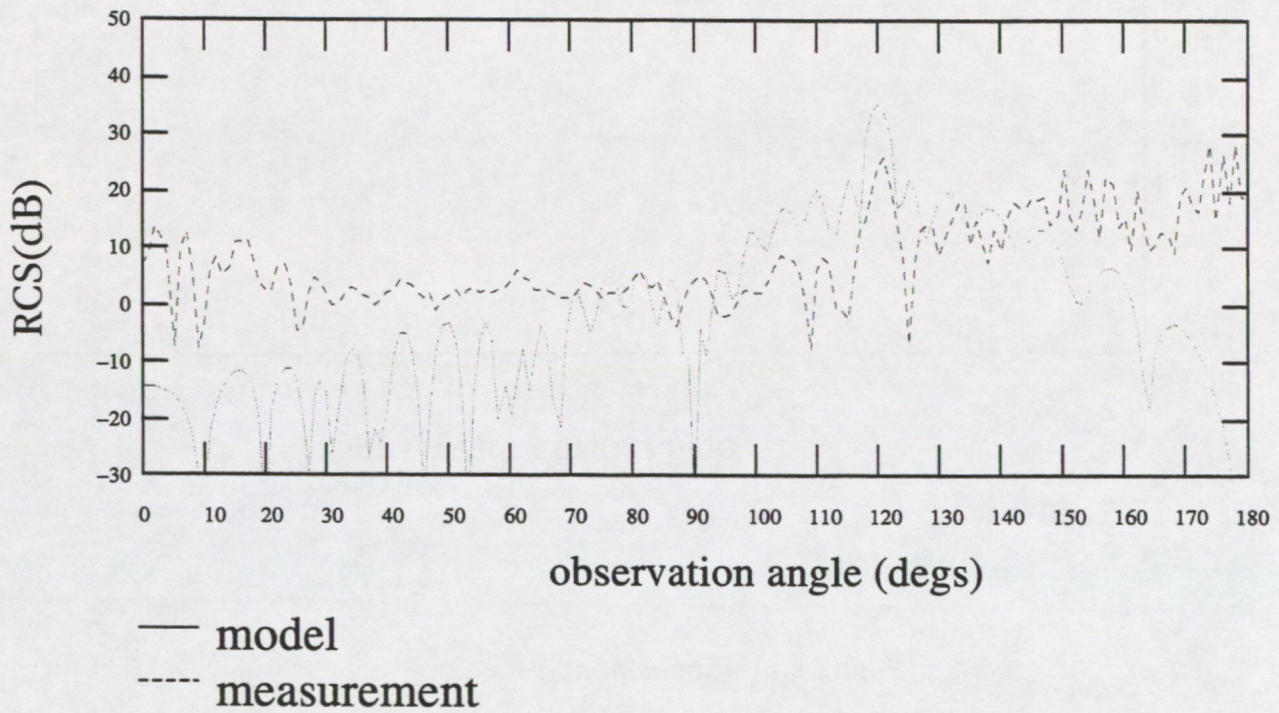


Figure 8(a) Incident angle = 60°

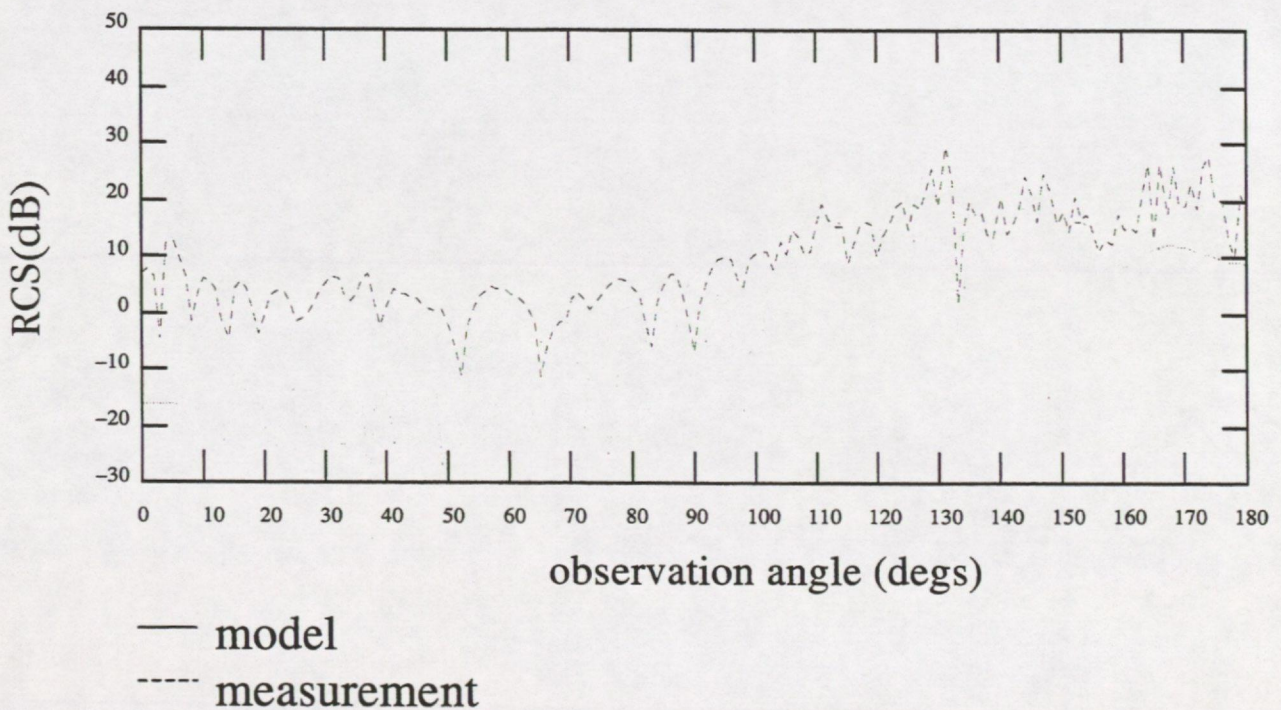


Figure 8(b) Incident angle = 50°

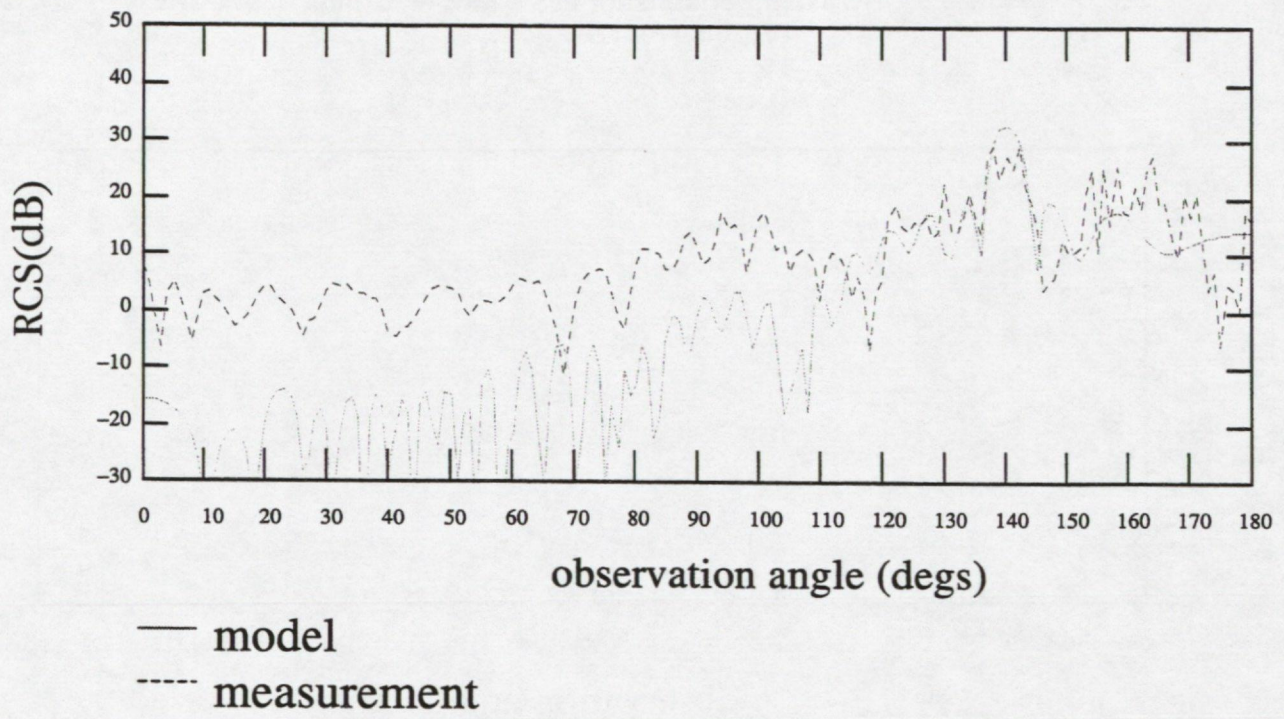


Figure 8(c) Incident angle = 40°

**Figure 9 RCS comparisons for scale model turbine at 5.0 GHz
(Vertical Polarisation)**

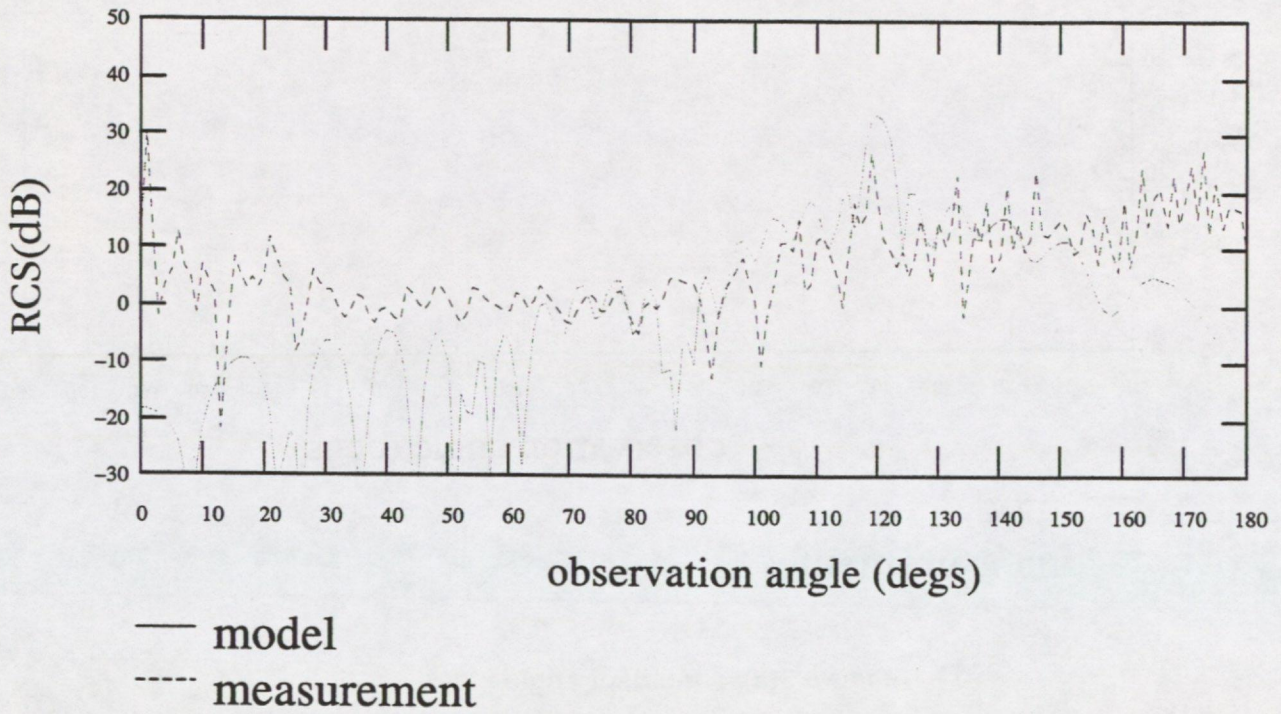


Figure 9(a) Incident angle = 60°

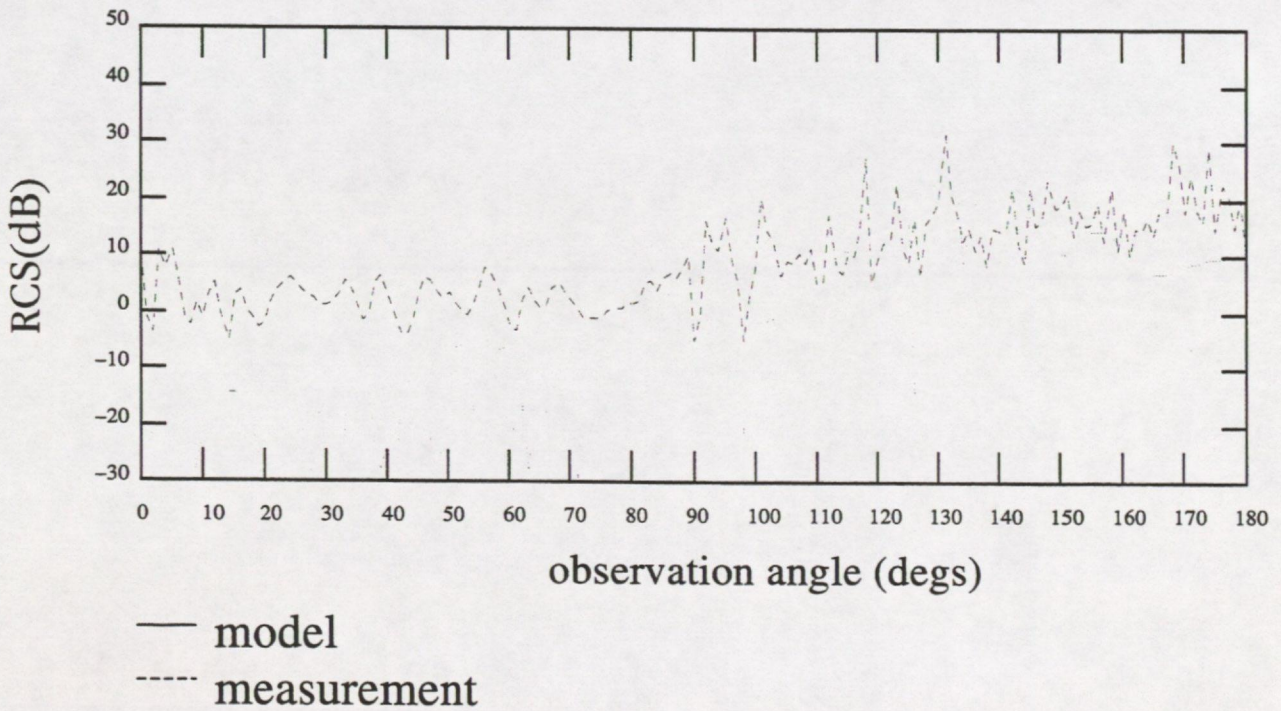


Figure 9(b) Incident angle = 50°

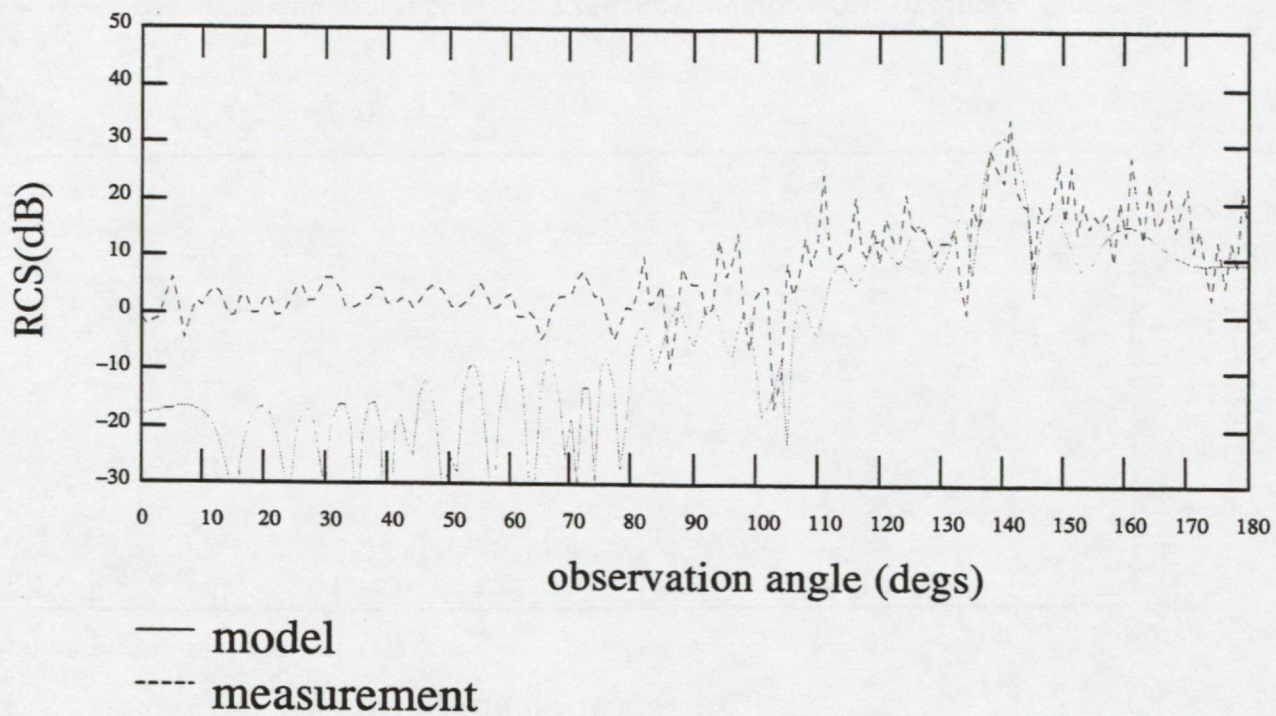


Figure 9(c) Incident angle = 40°

Figure 10 RCS comparisons for scale model turbine at 5.0 GHz
(Horizontal Polarisation)

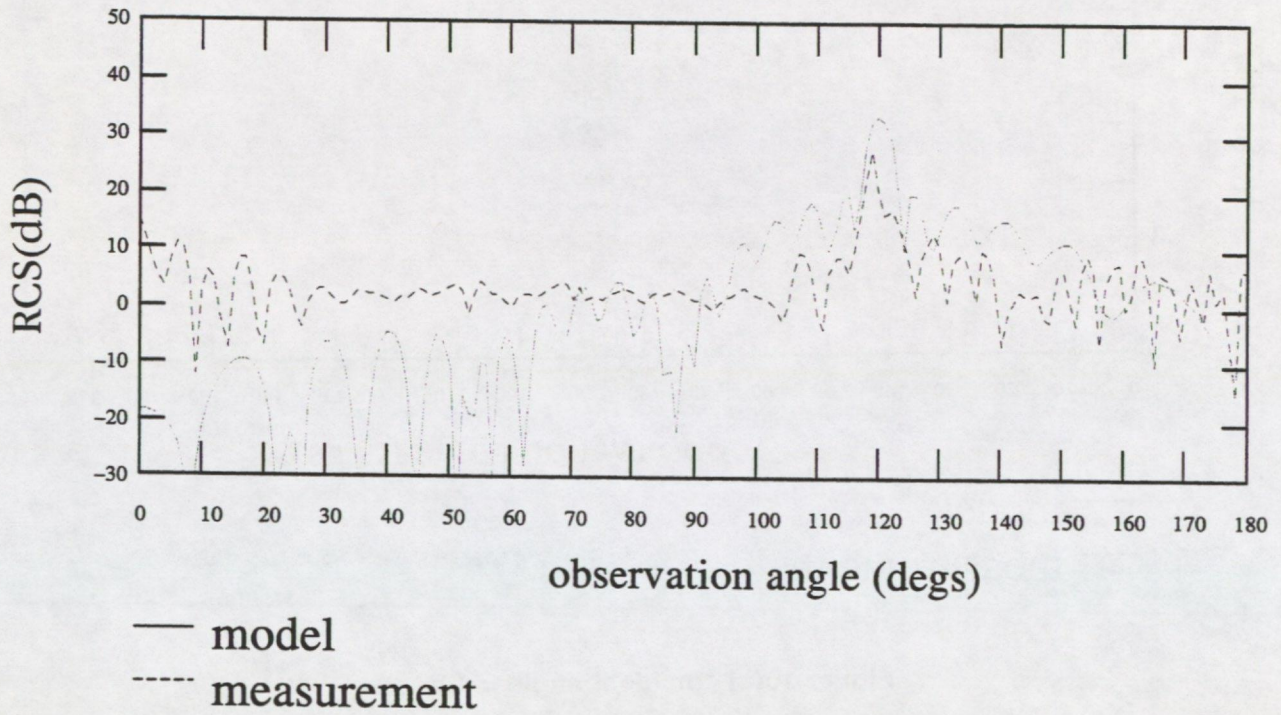


Figure 10(a) Incident angle = 60°

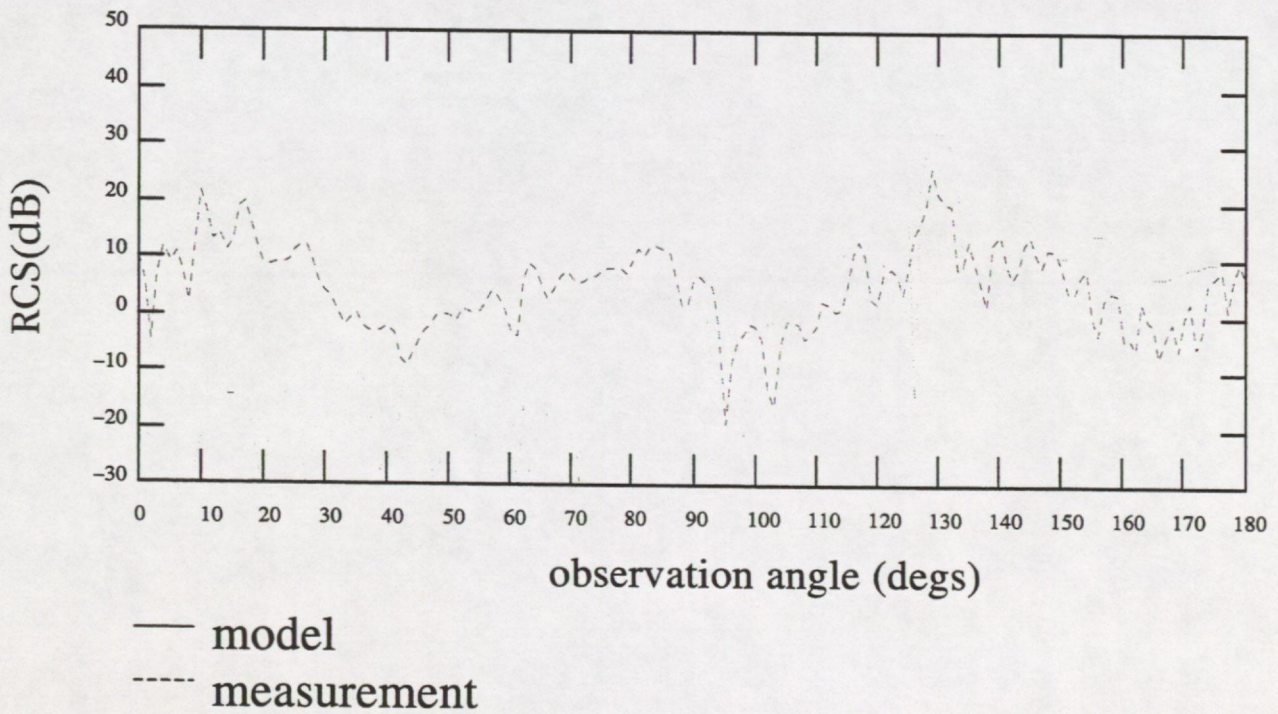


Figure 10(b) Incident angle = 50°

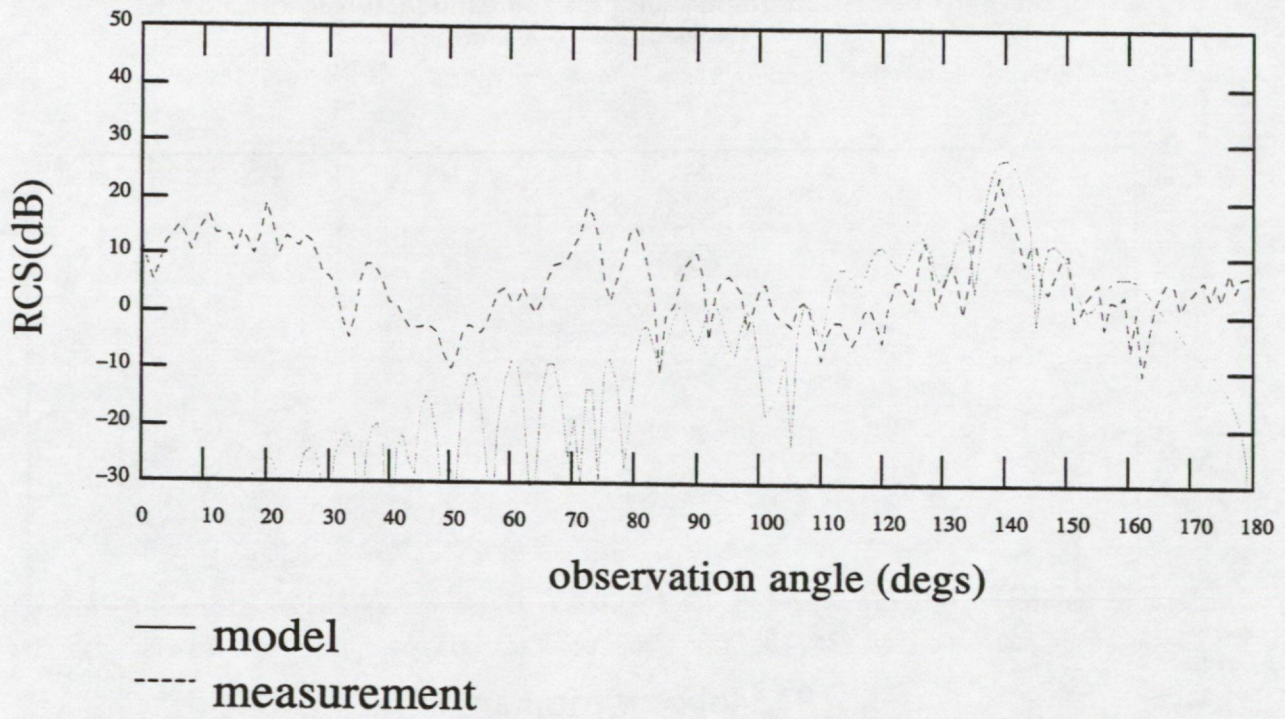


Figure 10(c) Incident angle = 40°

**Figure 11 RCS comparisons for scale model turbine at 3.2 GHz
(Vertical Polarisation)**

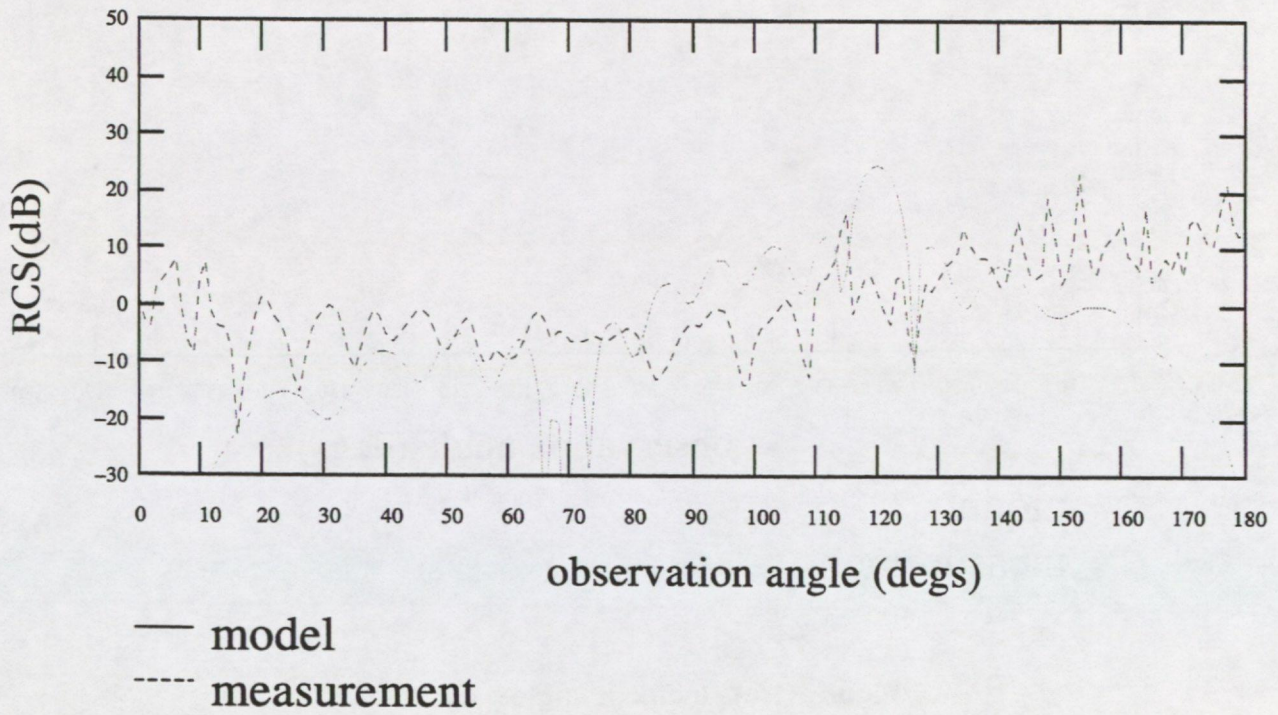


Figure 11(a) Incident angle = 60°

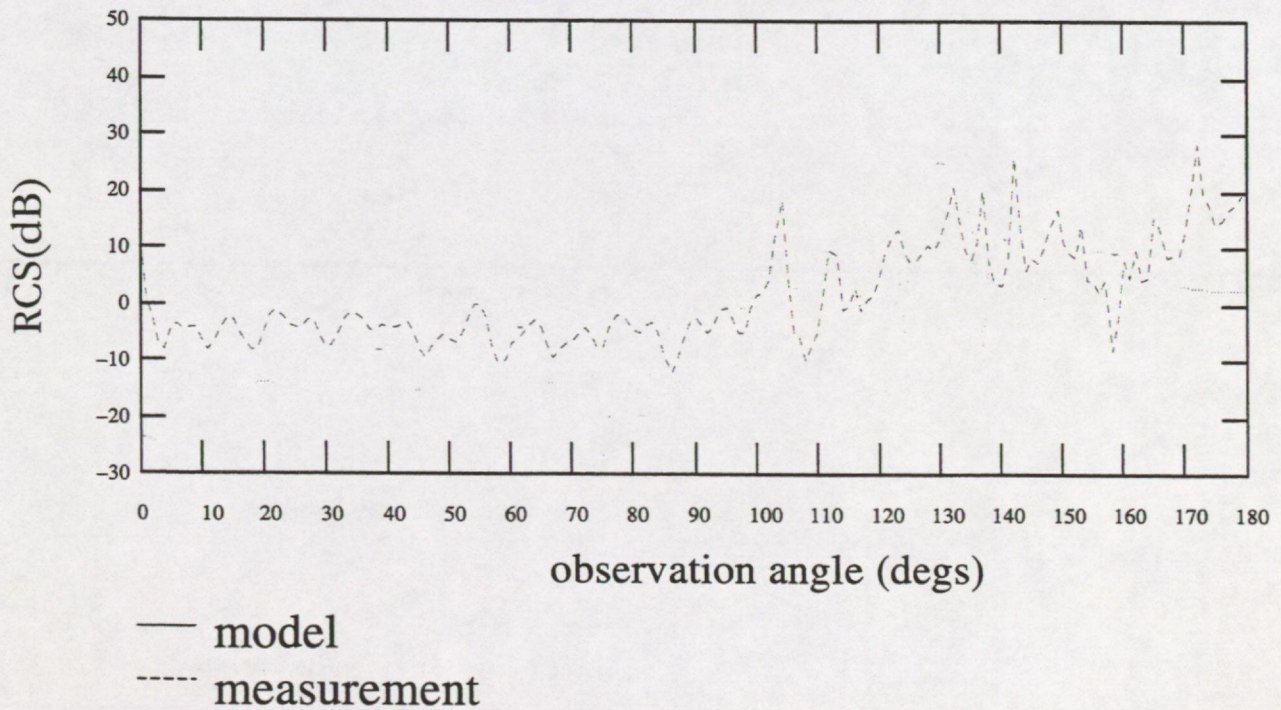


Figure 11(b) Incident angle = 50°

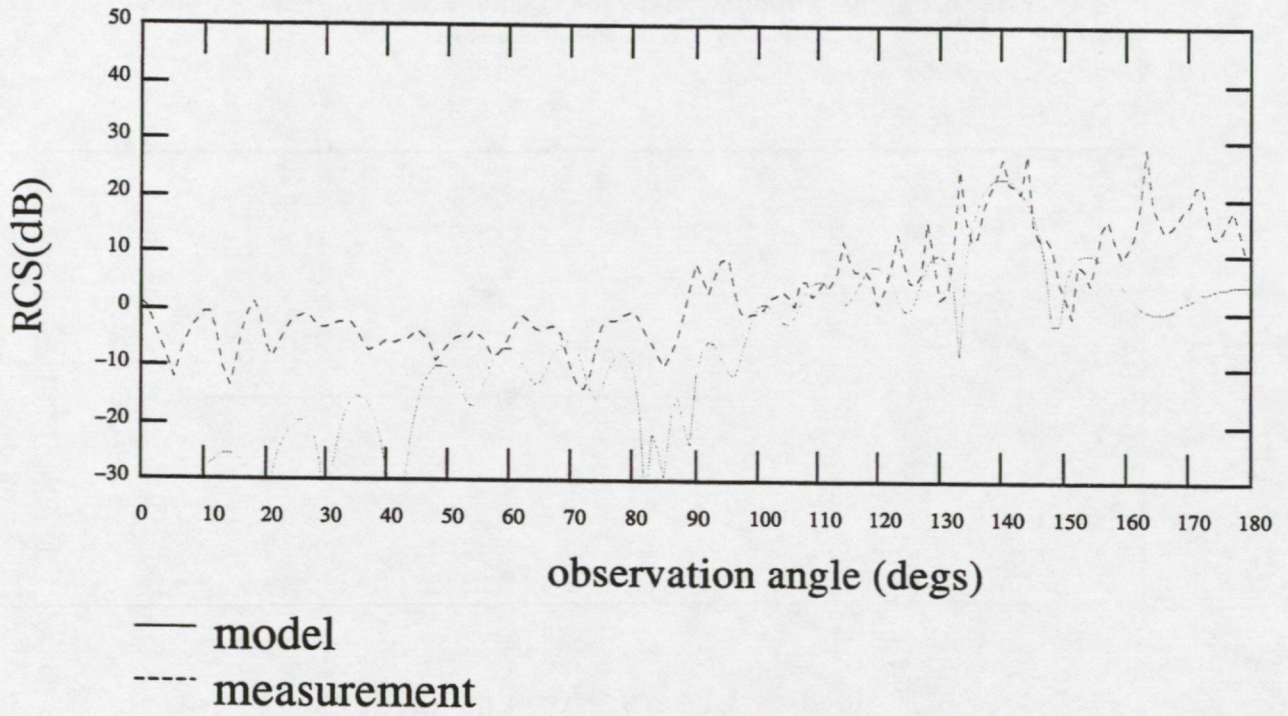


Figure 11(c) Incident angle = 40°

**Figure 12 RCS comparisons for scale model turbine at 3.2 GHz
(Horizontal Polarisation)**

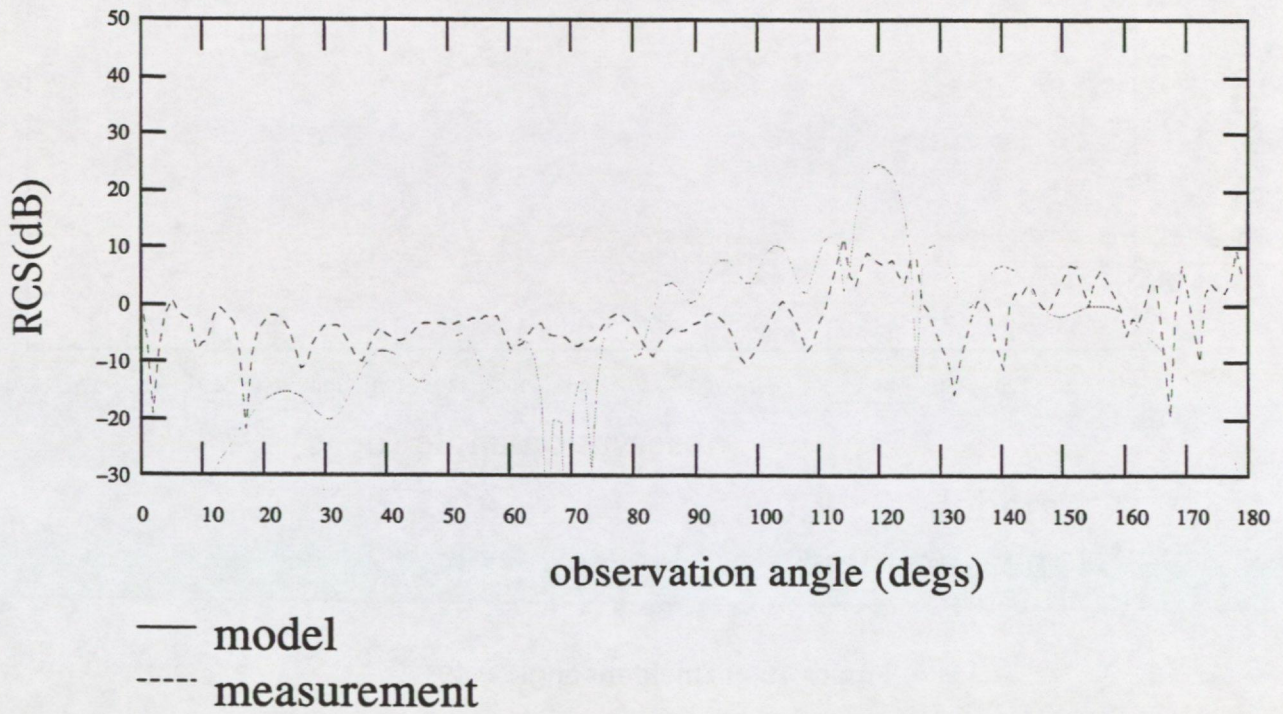


Figure 12(a) Incident angle = 60°

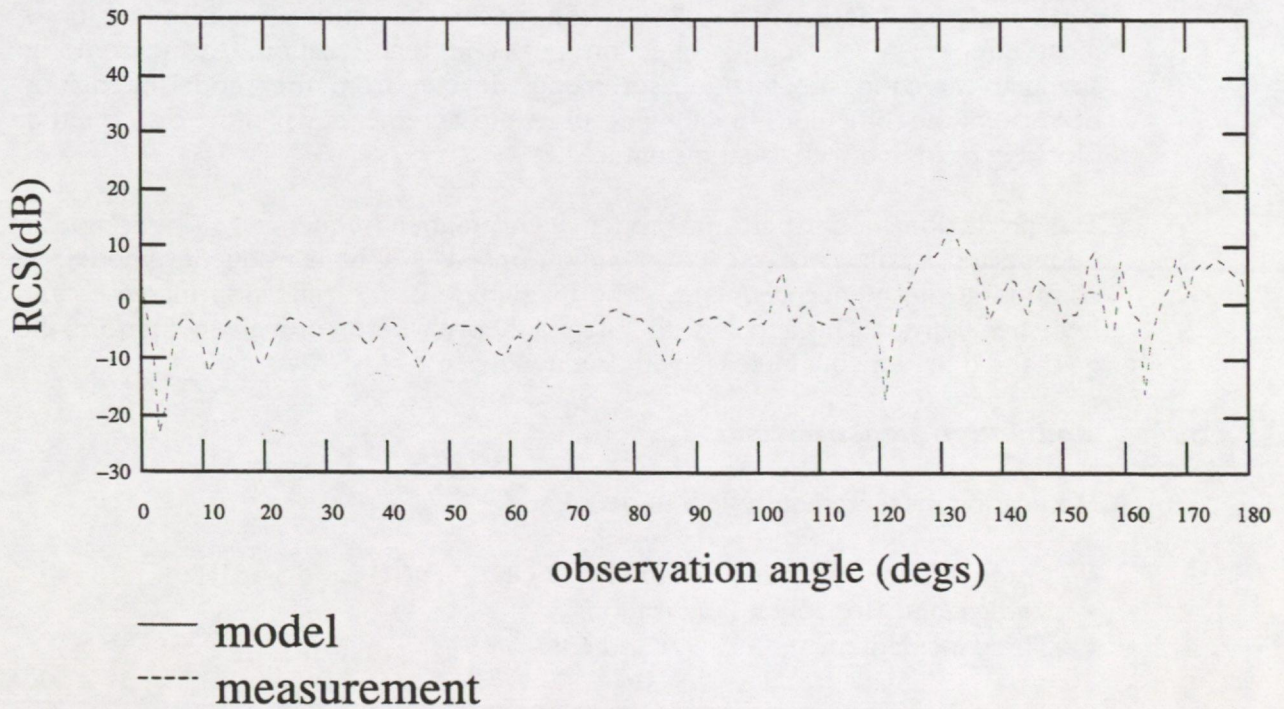


Figure 12(b) Incident angle = 50°

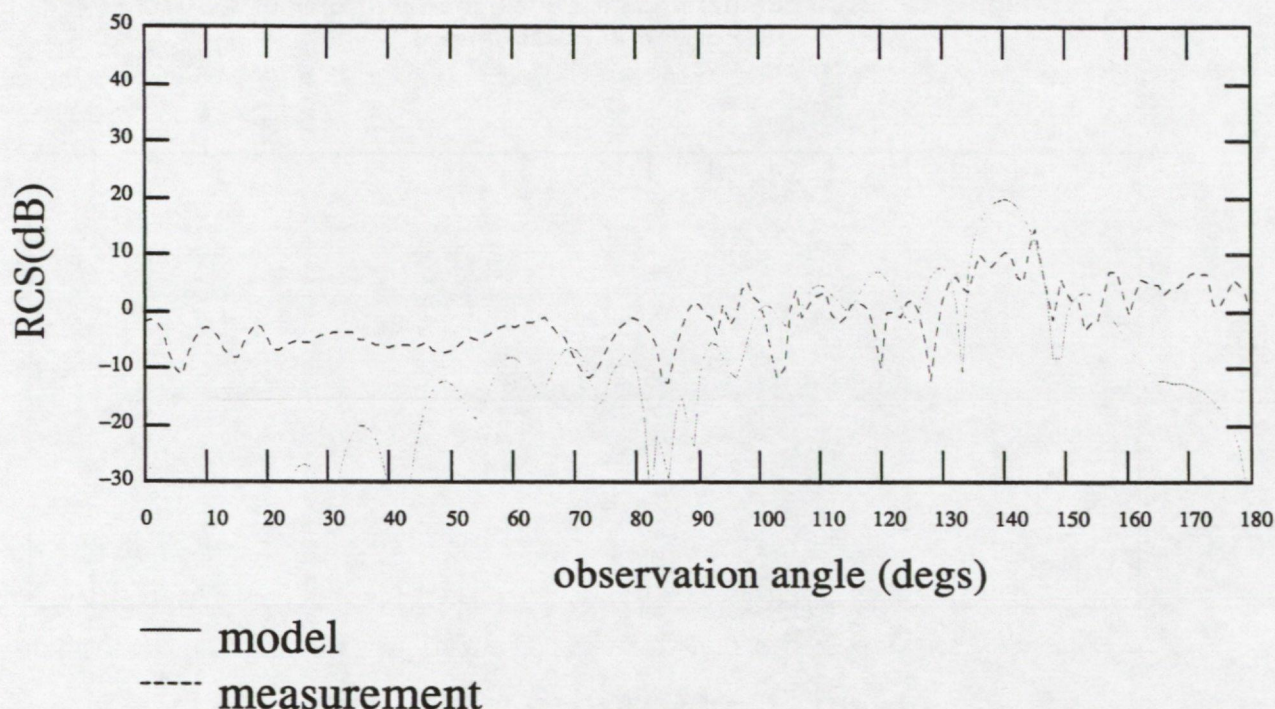


Figure 12(c) Incident angle = 40°

2.5.1.3 *Remarks on comparison results*

Agreement between the test results and model predictions is generally good particularly for measurements close to the specular direction. This is the region of most importance since the reflection peaks at that location. Away from the specular direction the test measurements deviate from the model prediction because of the difficulties in taking accurate measurements when the dish is either blocking or in line with the transmitter.

The prediction model performs better at the higher frequencies. This is not an unexpected result since the PO technique used is a high frequency model. In addition at the higher frequencies the magnitude of the reflection increases and becomes sharper. This agrees with antenna theory where, for a given aperture, the gain and directionality increase with frequency.

2.5.2 ***Modulation measurements***

Modulation measurements were undertaken for:

- Three different frequencies namely 3.2 GHz, 5.0 GHz and 5.5 GHz.
- Vertical and Horizontal Polarisation.
- Three incident angles 40°, 50° and 60°.

The modulation was measured at 10° intervals of the observation angle. The rotation speed of the blades was set to 30 rpm which is close to the rotation speed of a typical wind turbine (34 rpm). Exact speeds are not required since the objective of these tests was to find the general trends in the data.

The region of most interest for verification is that at or near the specular direction. Although not shown in the figures that follow, both the prediction model and the test measurements confirm that no modulation occurs at the specular direction. This may be explained by consideration of the RCS results. At the specular direction maximum reflection occurs. This corresponds to the maximum area that the turbine projects towards the observation point and this will stay constant at the various blade locations hence producing no modulation waveform.

Near the specular direction, however, amplitude modulation exists. Although not constant, the modulation may be mathematically described by a repetitive sinc function where $\text{sinc}(x) = \sin(x)/x$. The frequency of repetition of the waveform is closely related to the frequency of the rotation of the blades themselves. Fourier transforming the modulation waveform reveals that the first frequency component is equal to three times the frequency of the blade rotation. The spectrum also shows that higher order harmonics are present in the waveform.

The normal operational rotation of some models of wind turbine is 34 rpm. Since in these tests, the blades' rotation was set to 30 rpm, it is expected that in a real situation, the modulation frequencies will be slightly higher.

The modulation index is an important parameter as it gives an indication of the depth of the modulation. It is defined as the ratio of the maximum to minimum value in the modulated signal. The modulation index can be calculated using the following:

$$20 \log_{10} \left(\frac{1+m}{1-m} \right) = \Delta_1 - \Delta_2$$

where Δ_1 and Δ_2 are the field strength deviations above and below the ambient level. For the example in Figure 13 (a) these are 2 dB and -12 dB respectively yielding $m = 0.66$. Table 2.1 shows the modulation index variation at various parameter settings.

Table 2.1 Modulation index for various parameters (Incident angle 60°)

<i>Observation angle</i>	<i>Frequency (GHz)</i>	<i>Modulation Index</i>
100°	5.5	0.66
140°	5.5	0.78
100°	5.0	0.85
140°	5.0	0.89
100°	3.2	0.66
140°	3.2	0.69

Figures 13–19 show comparisons between the results predicted by the model and the test results.

Figure 13

Modulation results
Incident angle = 60° , Observation = 100° ,
Horizontal Polarisation, 5.5 GHz

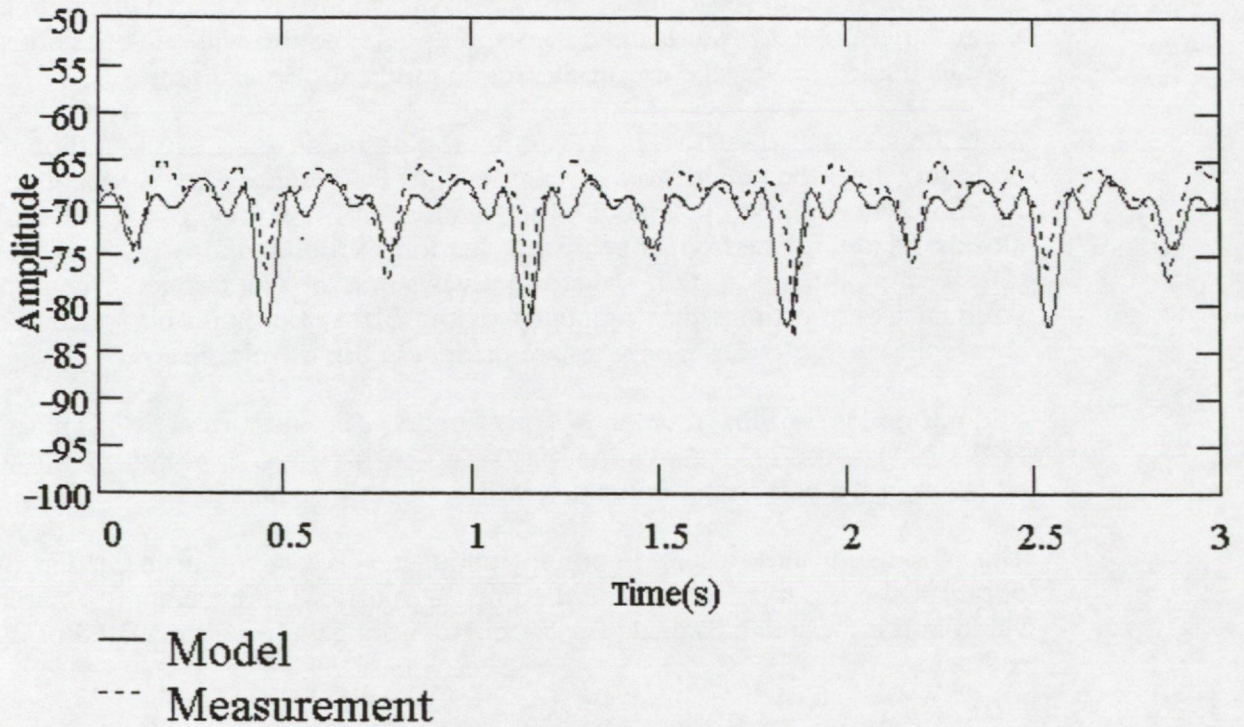


Figure 13(a) Time waveform comparison

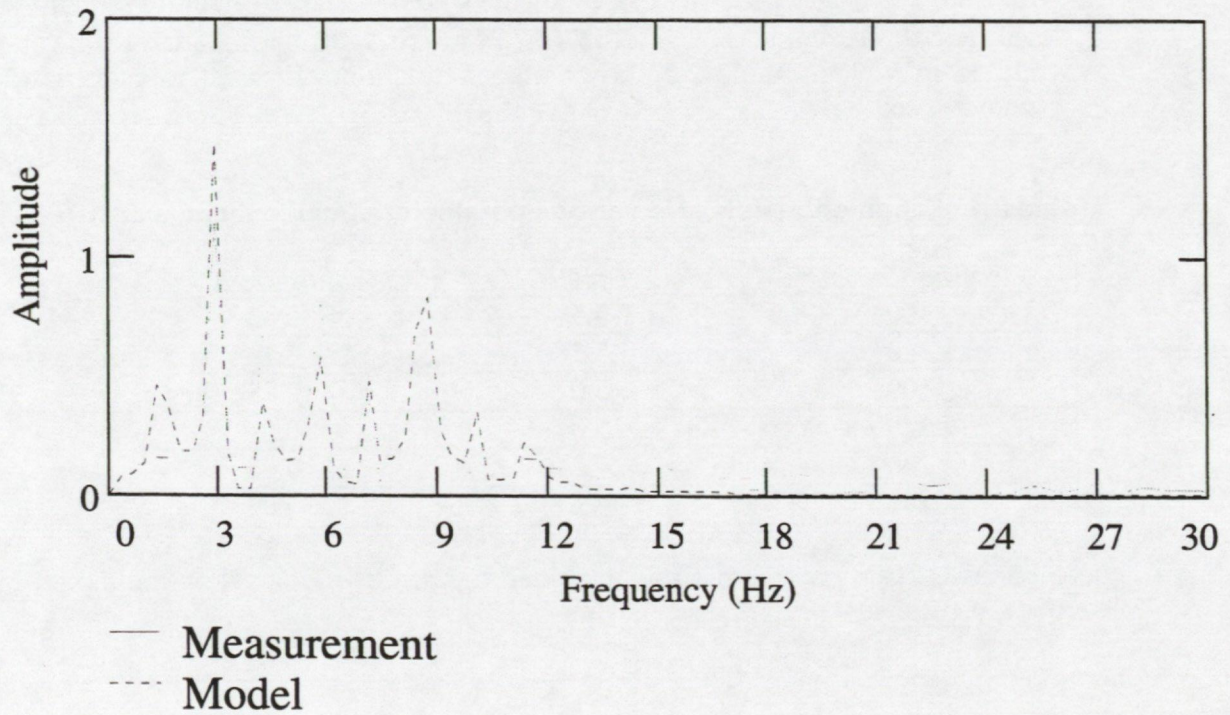


Figure 13(b) Spectrum comparison

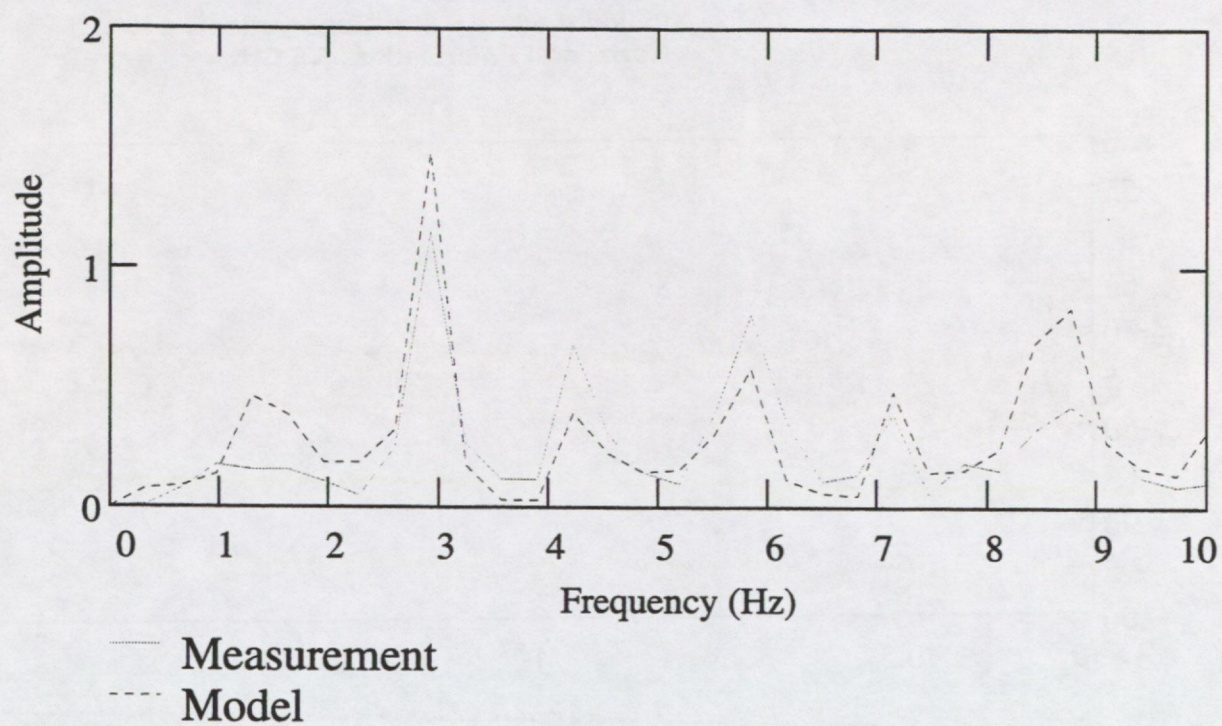


Figure 13 (c) Spectrum comparison

Figure 14 Modulation results
Incident angle = 60° , Observation = 140° ,
Horizontal Polarisation, 5.5 GHz

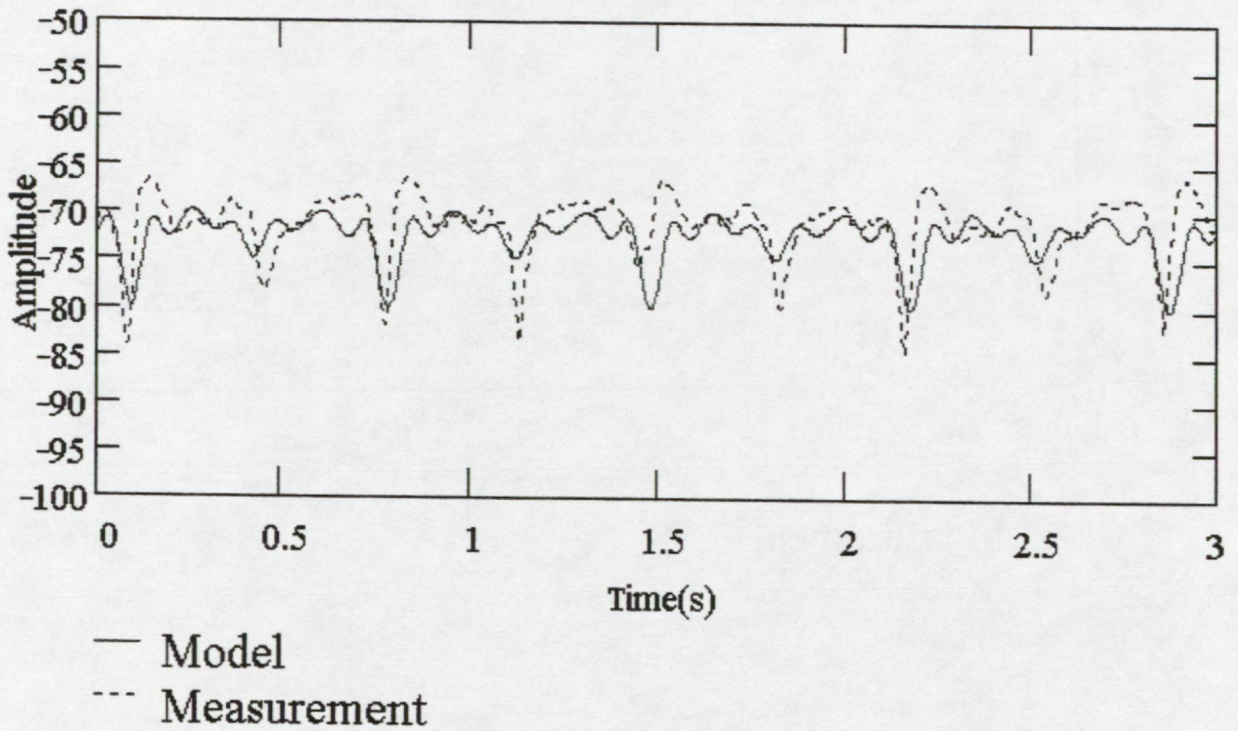


Figure 14(a) Time waveform comparison

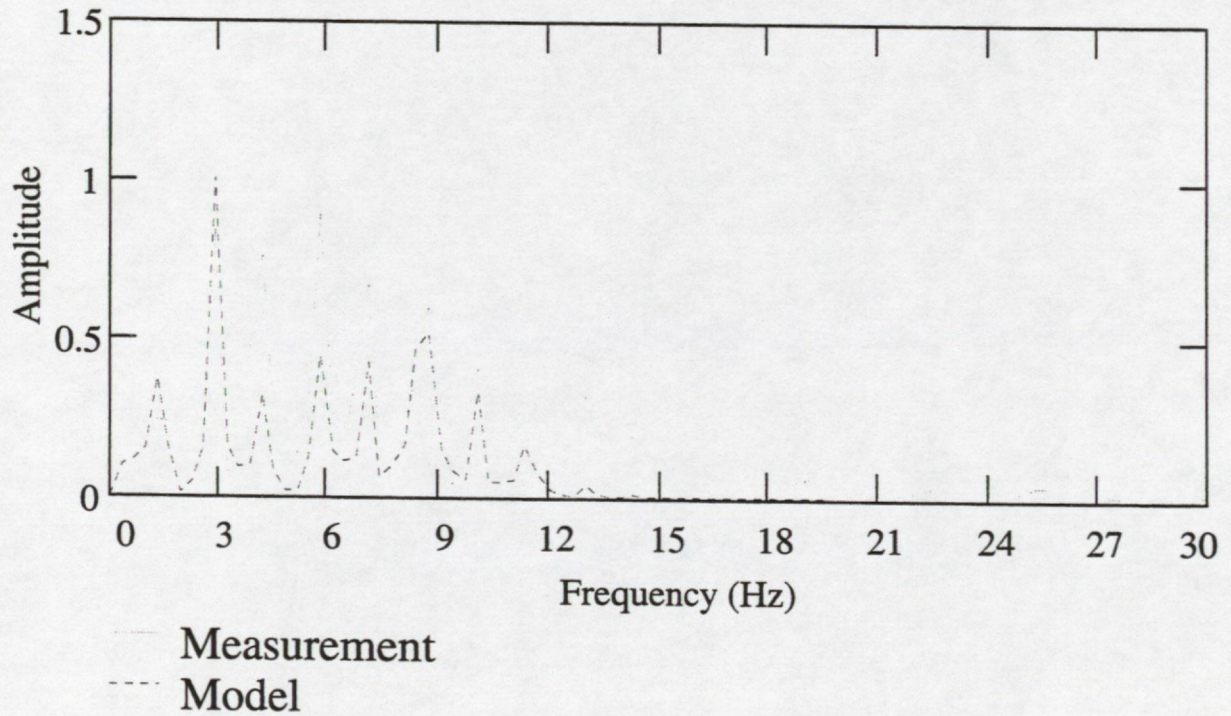


Figure 14(b) Spectrum comparison

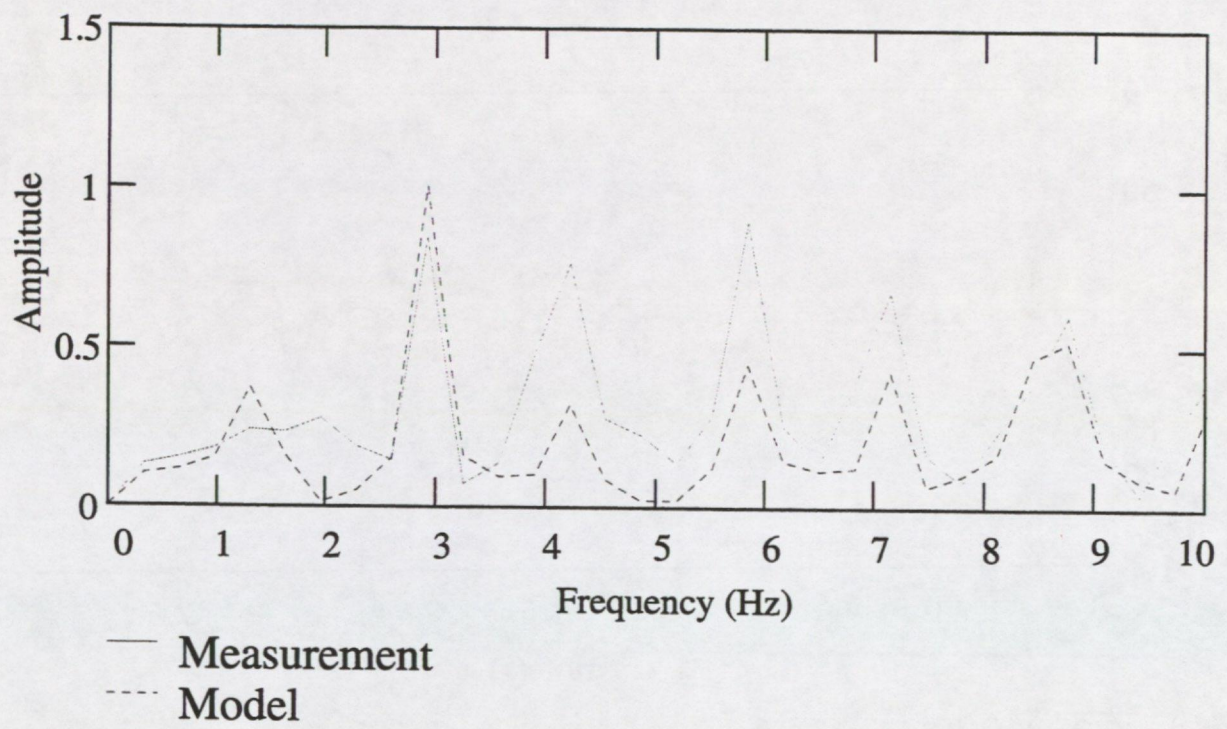


Figure 14(c) Spectrum comparison

Figure 15 Modulation results
Incident angle = 60° , Observation = 150° ,
Horizontal Polarisation, 5.5 GHz

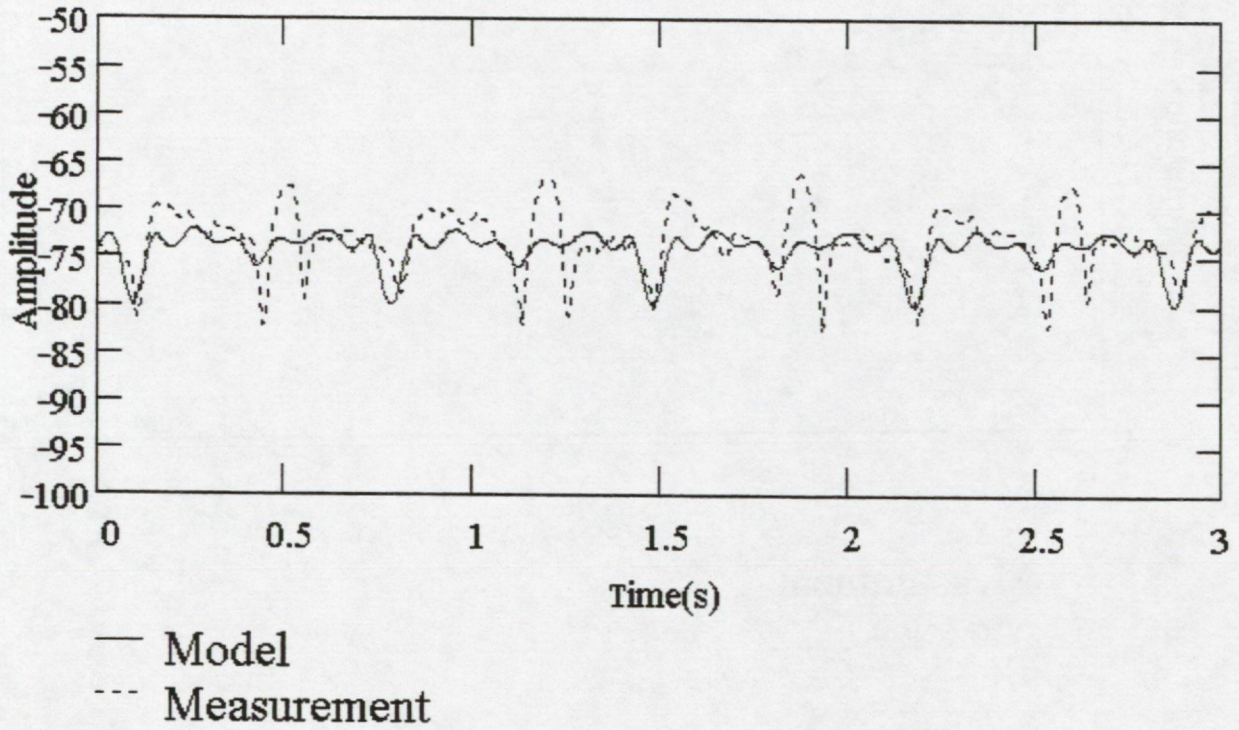


Figure 15(a) Time waveform comparison

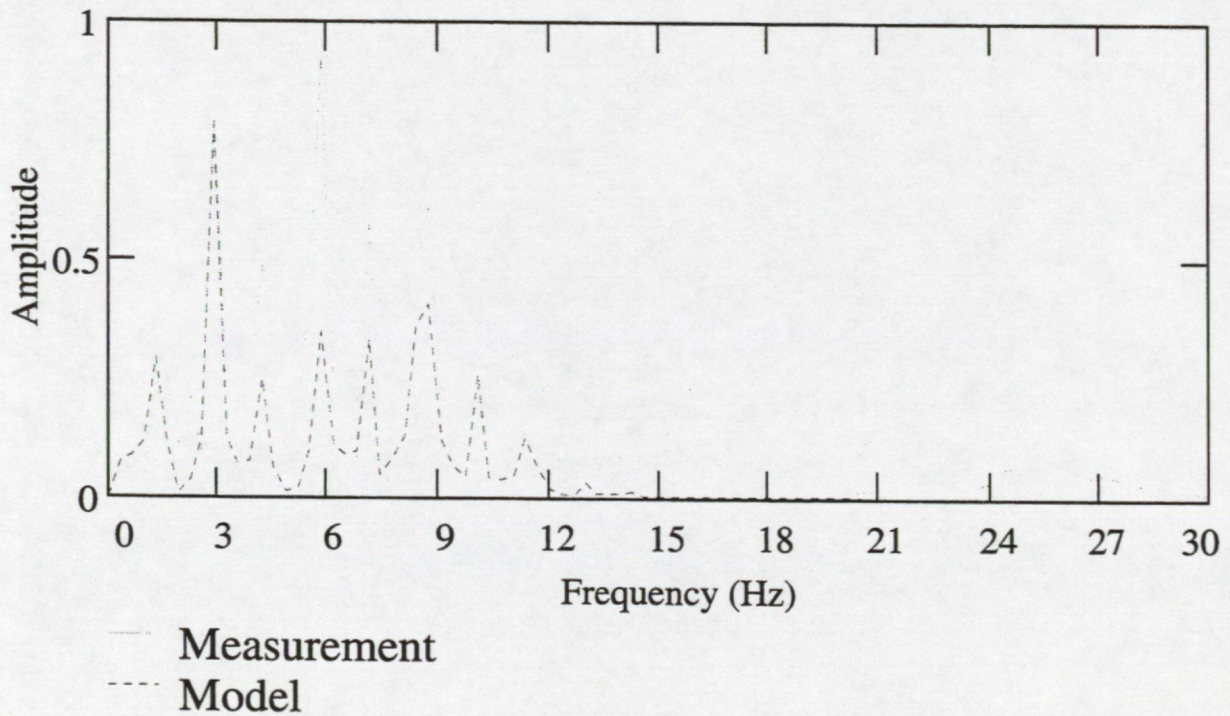


Figure 15(b) Spectrum comparison

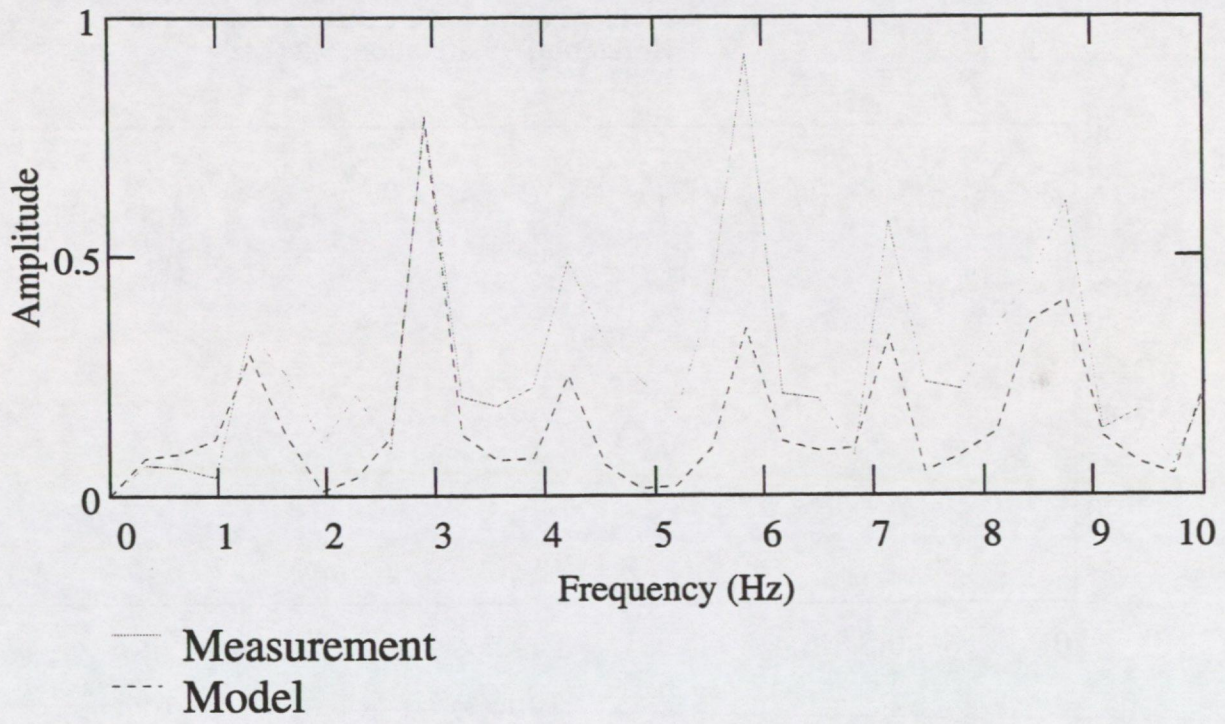


Figure 15(c) Spectrum comparison

Figure 16 Modulation results
Incident angle = 60° , Observation = 100° ,
Horizontal Polarisation, 5.0 GHz

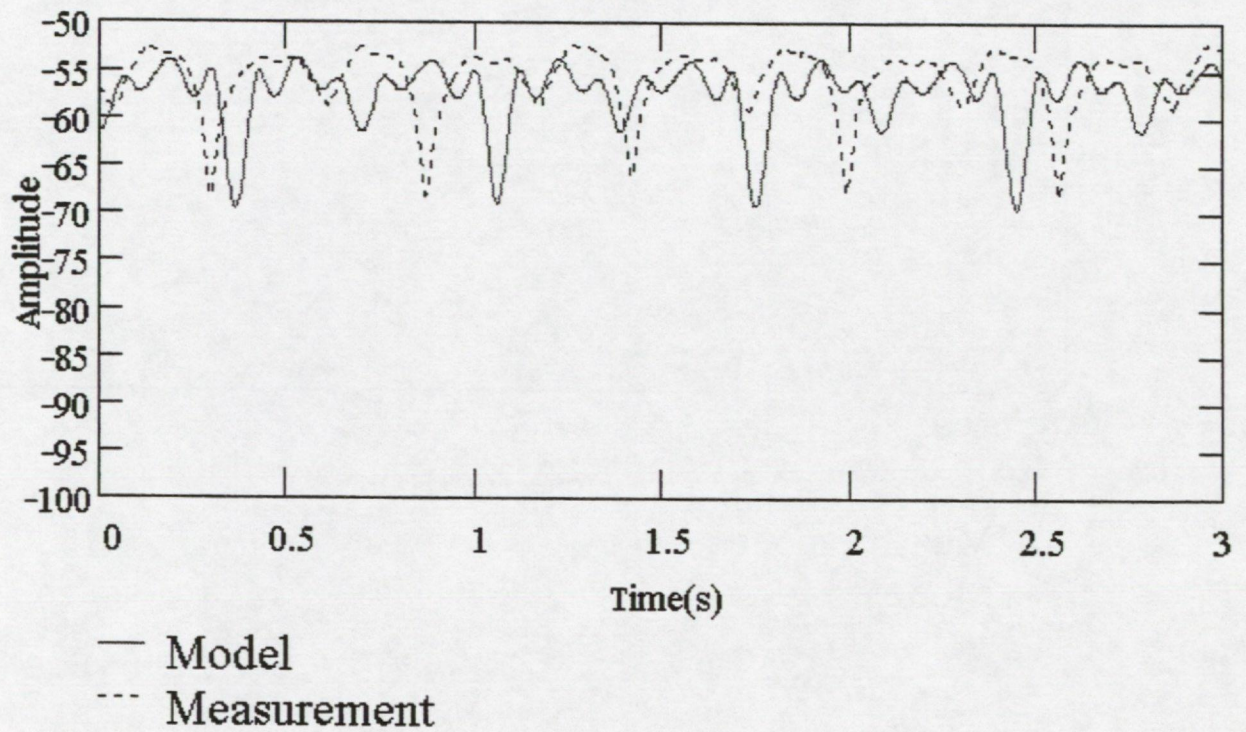


Figure 16(a) Time waveform comparison

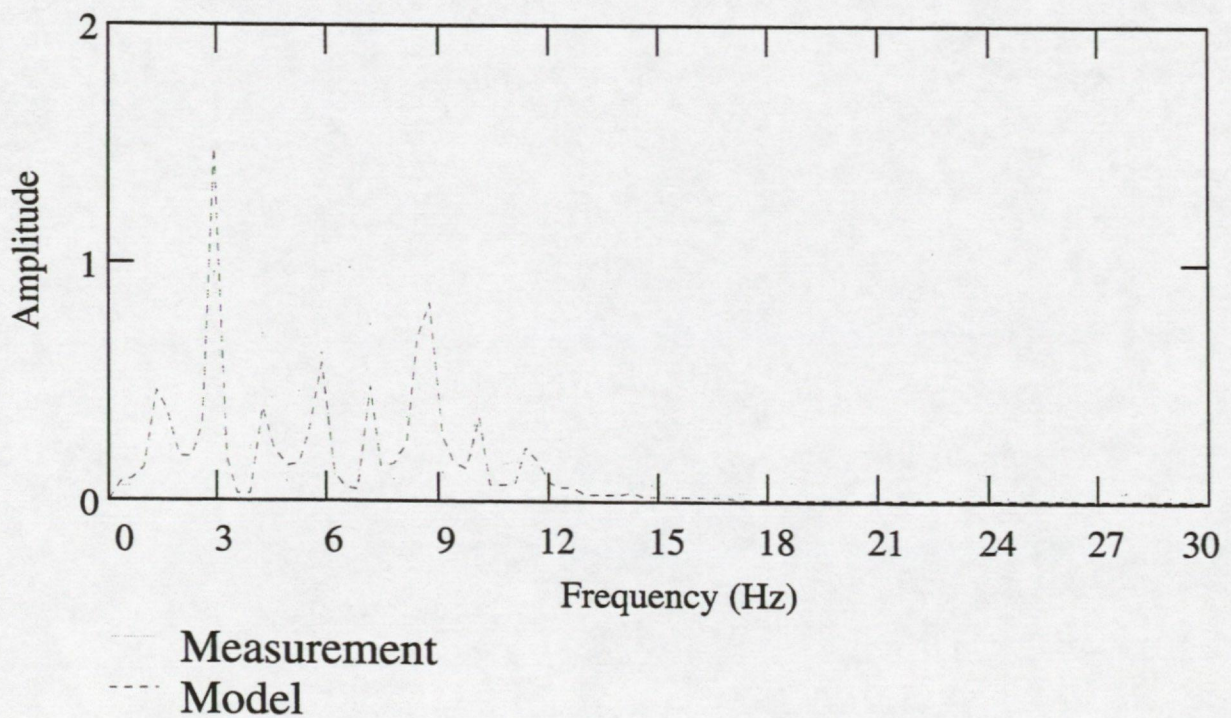


Figure 16(b) Spectrum comparison

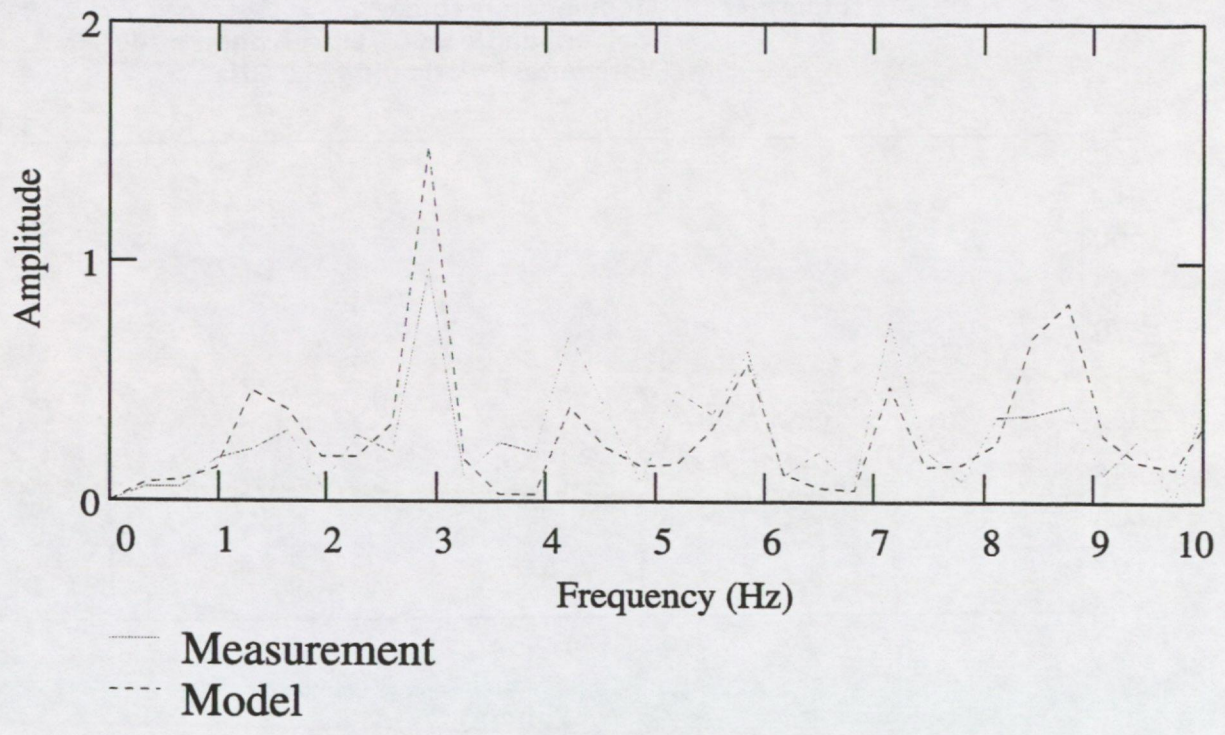


Figure 16(c) Spectrum comparison

Figure 17 Modulation results
Incident angle = 60° , Observation = 140° ,
Horizontal Polarisation, 5.0 GHz

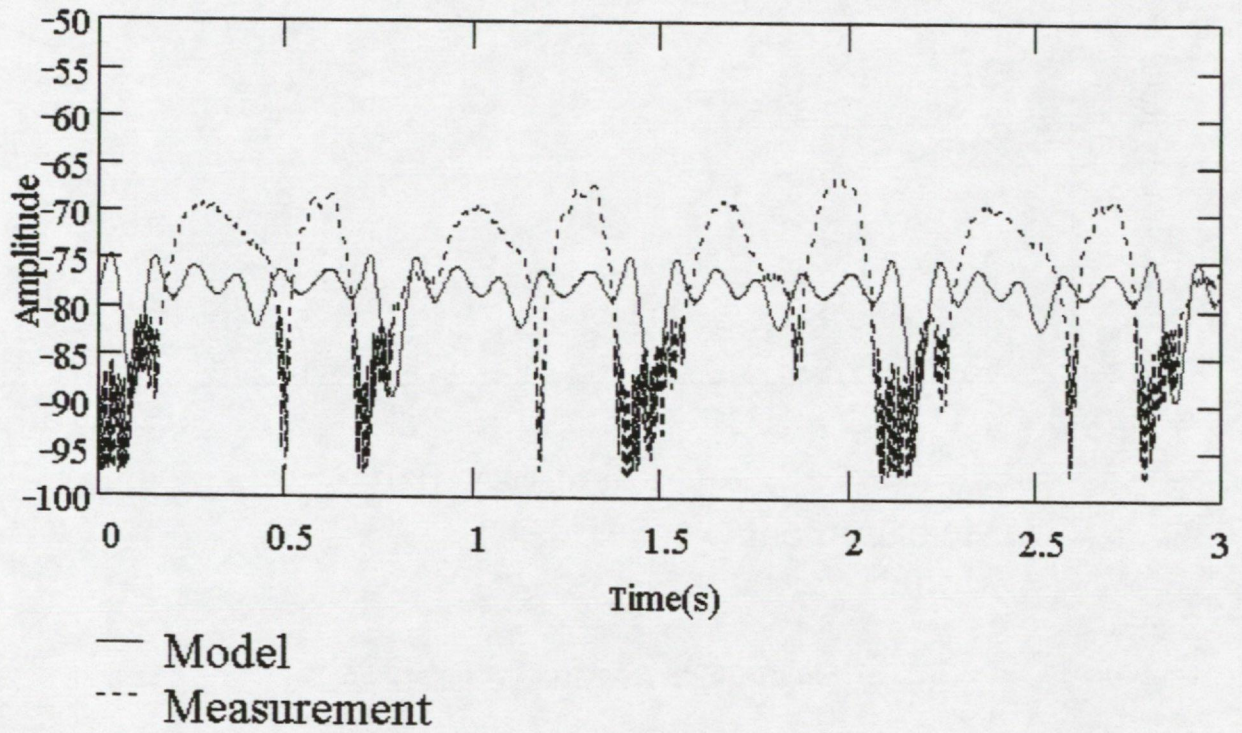


Figure 17(a) Time waveform comparison

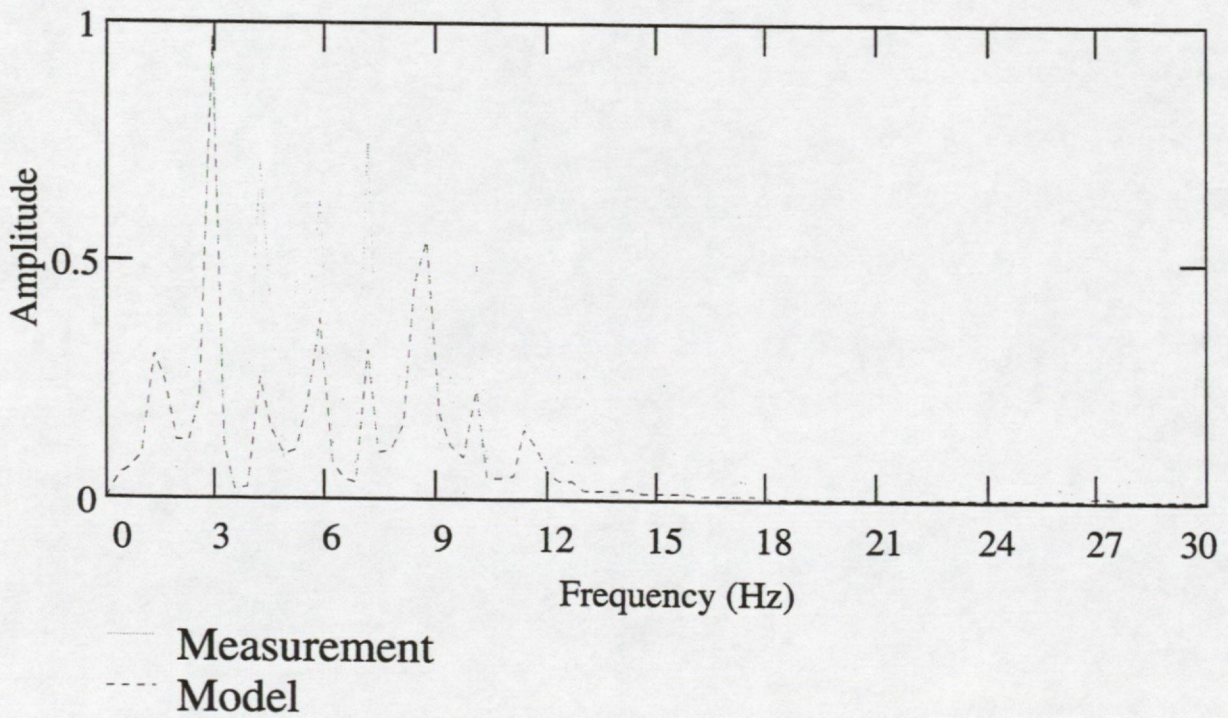


Figure 17(b) Spectrum comparison

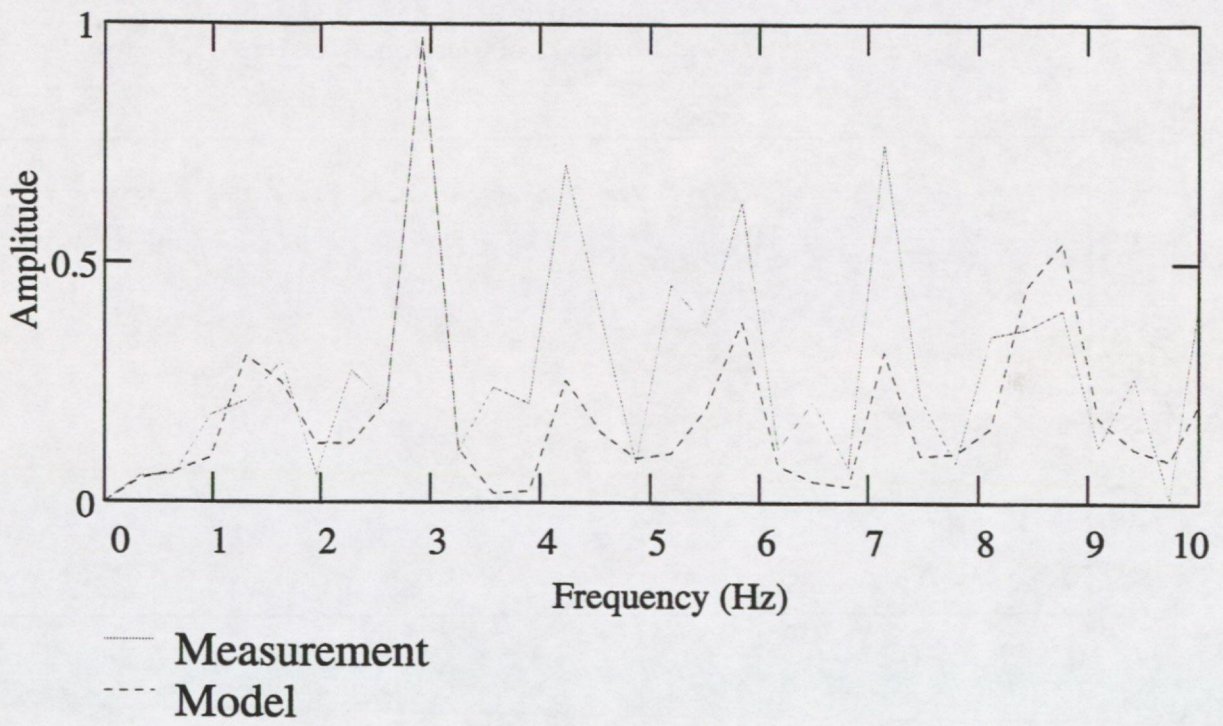


Figure 17(c) Spectrum comparison

Figure 18 Modulation results
Incident angle = 60° , Observation = 100° ,
Vertical Polarisation, 3.2 GHz.

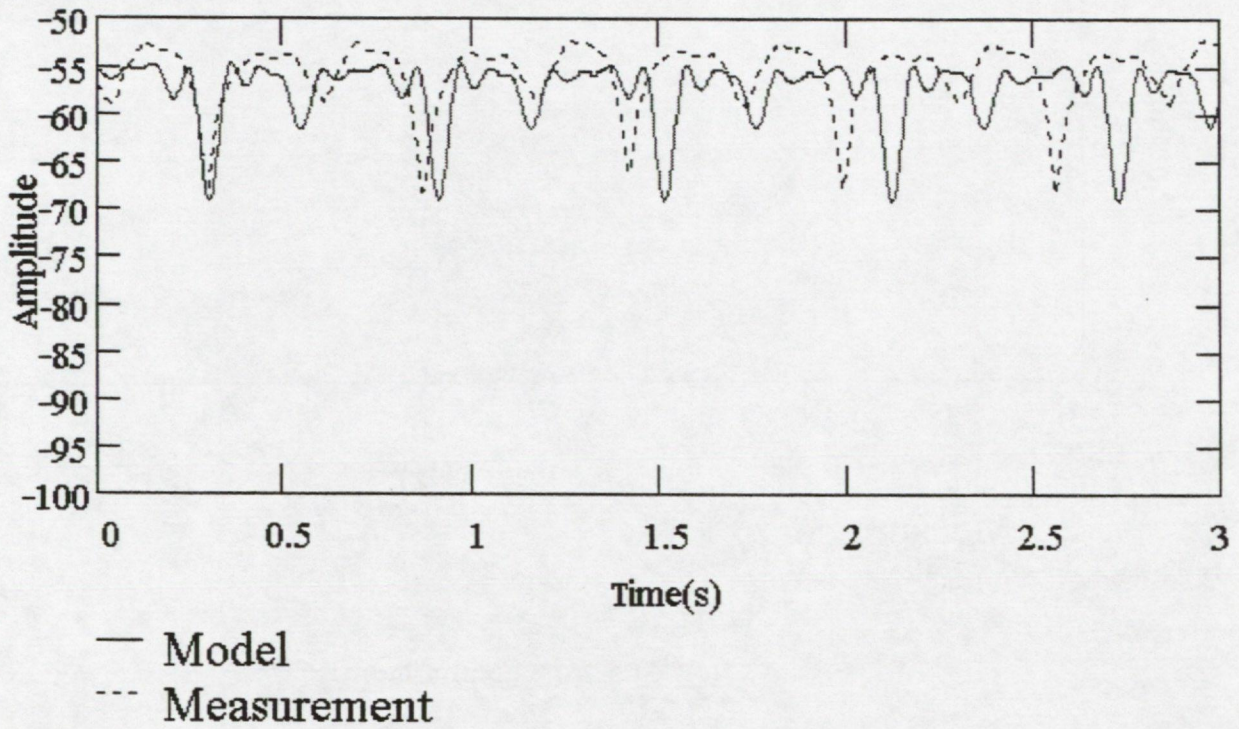


Figure 18(a) Time waveform comparison

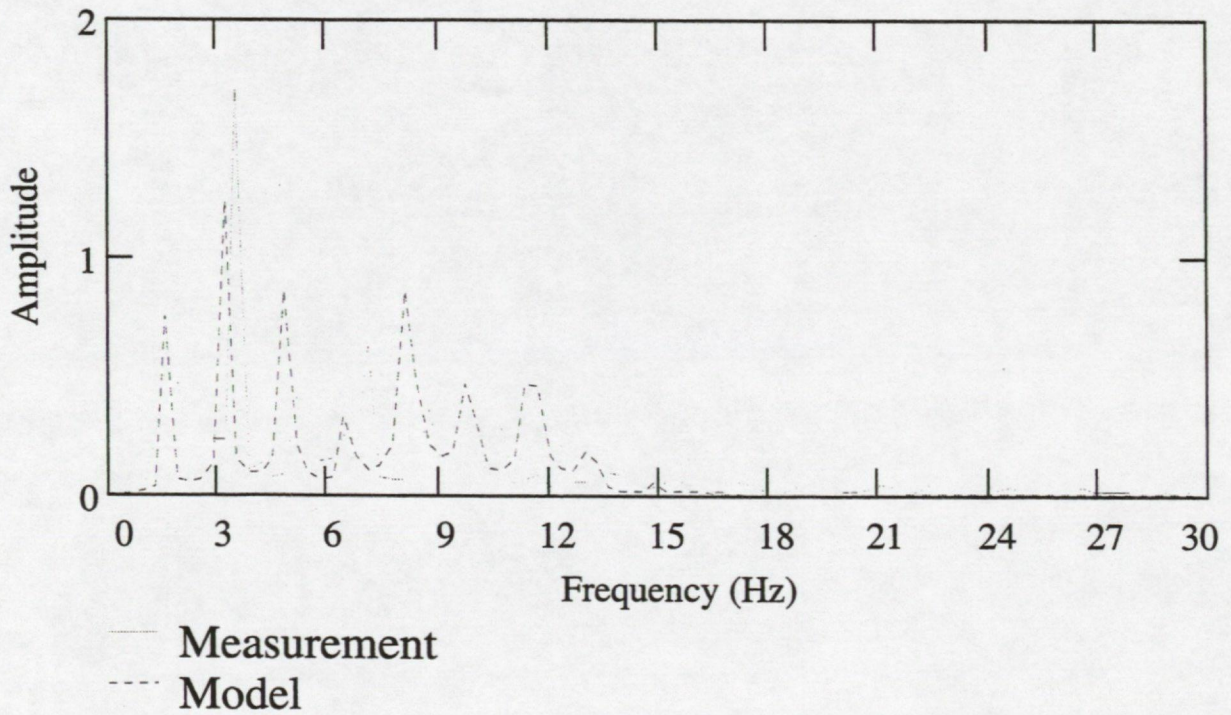


Figure 18(b) Spectrum comparison

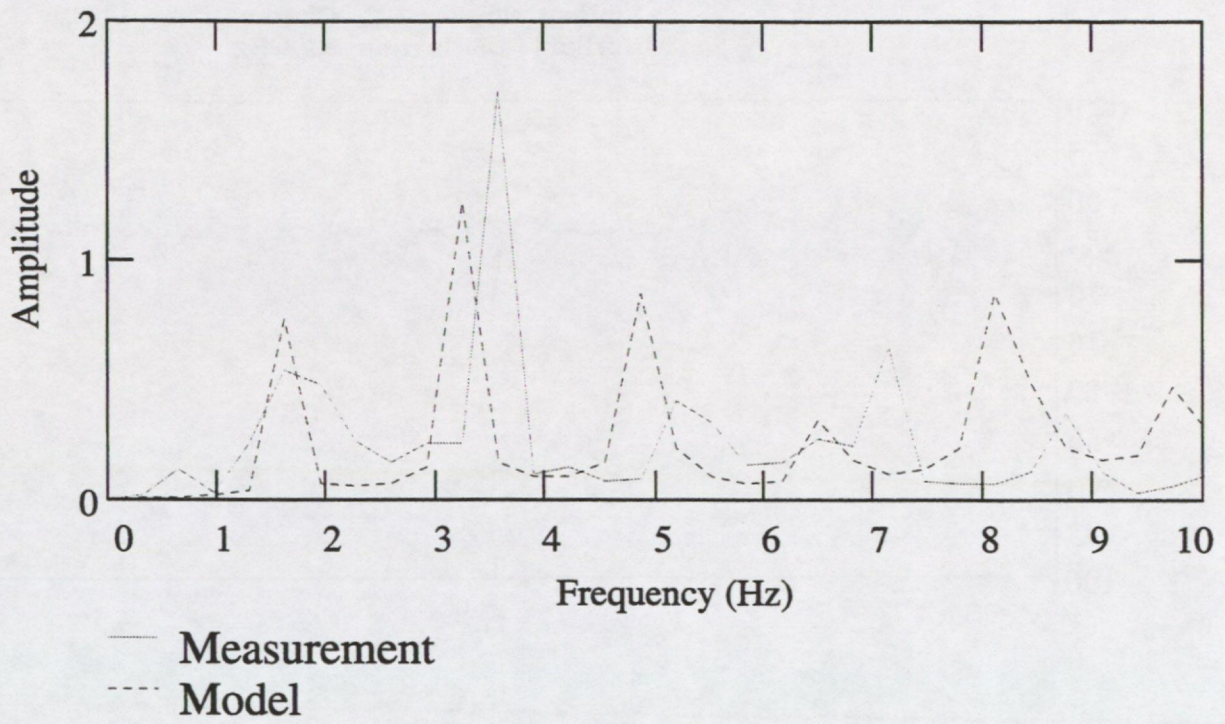


Figure 18(c) Spectrum comparison

Figure 19

Modulation results
Incident angle = 60° , Observation = 140° ,
Vertical Polarisation, 3.2 GHz.

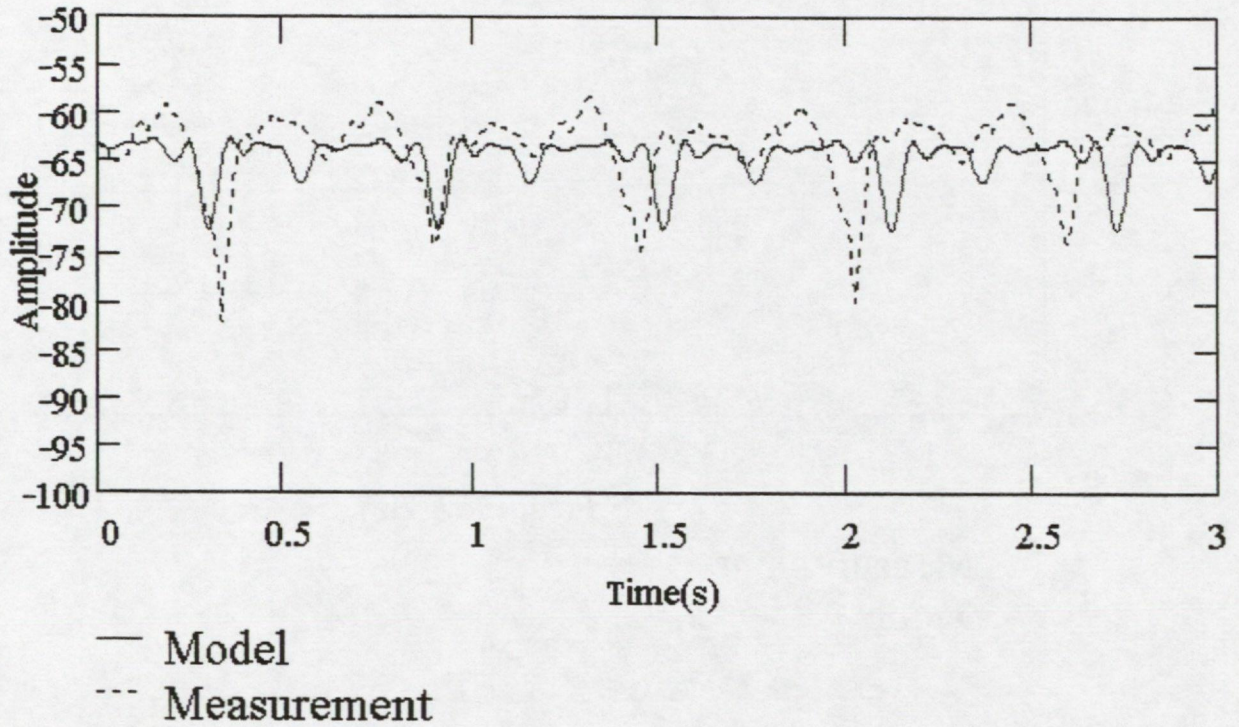


Figure 19(a) Time waveform comparison

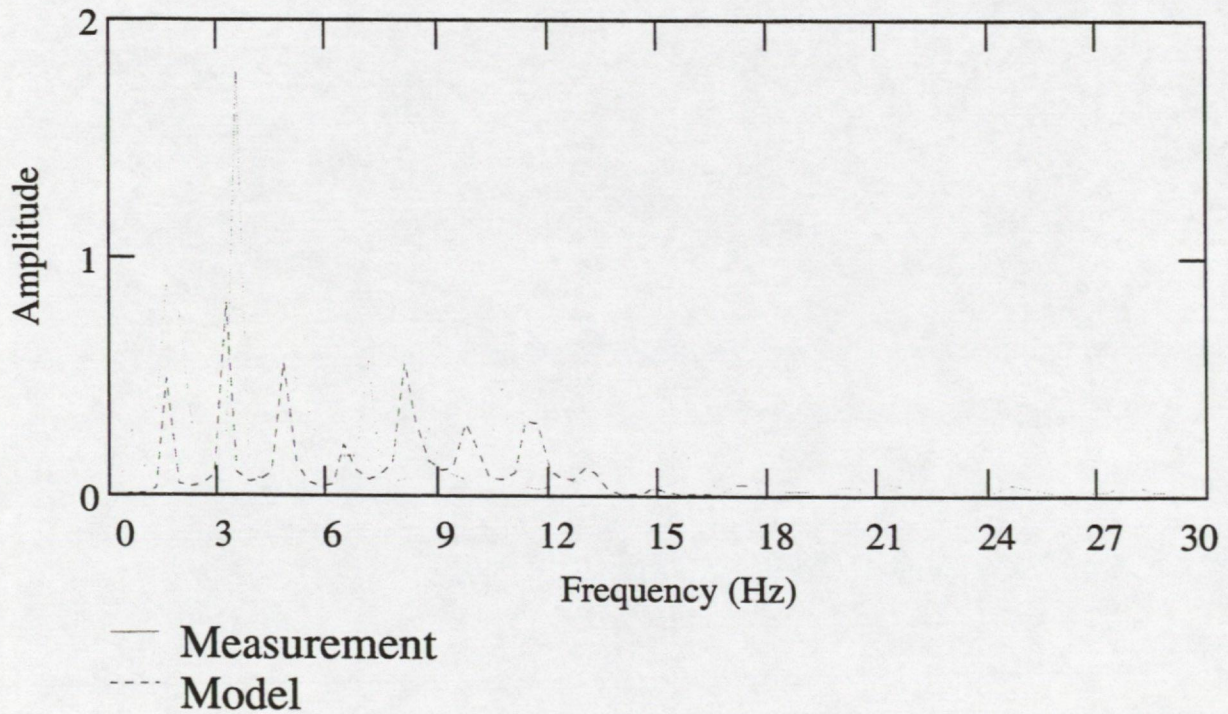


Figure 19(b) Spectrum comparison

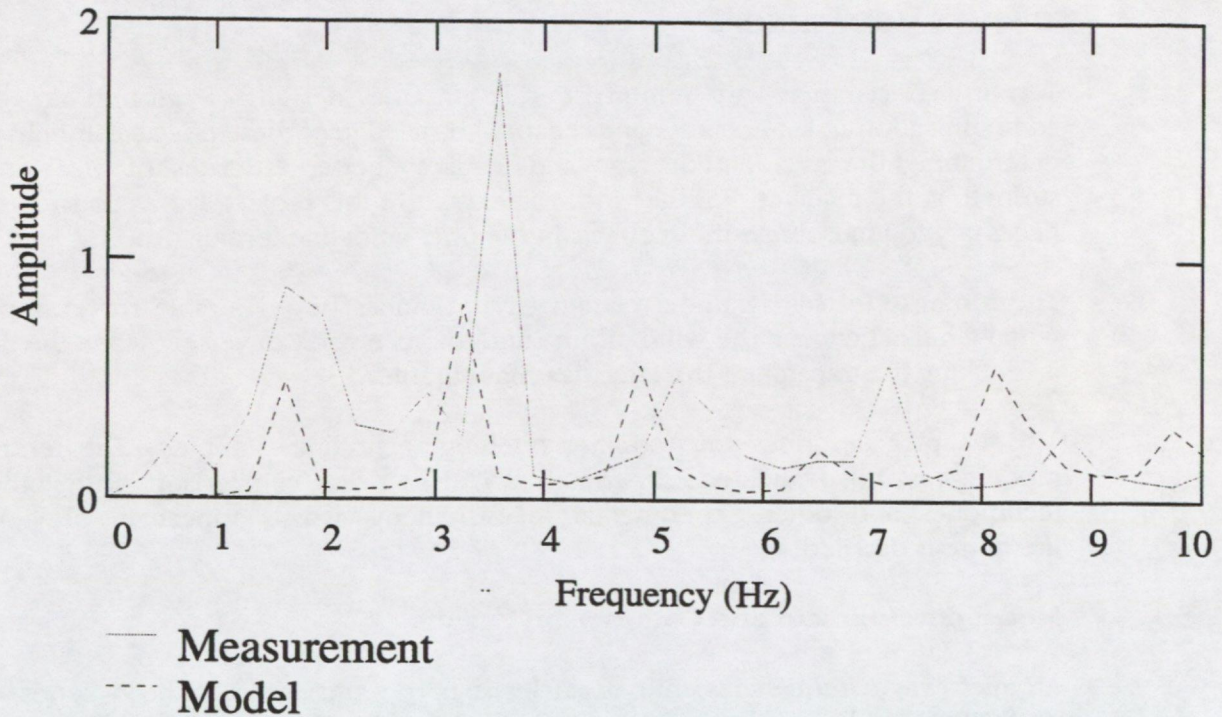


Figure 19(c) Spectrum comparison

2.5.2.1 *Remarks on Modulation Results*

The model predictions show close agreement with the test measurements both in the time and frequency domains. As with the RCS measurements there were difficulties in making accurate measurements in the directions in line with the transmitter.

Observations of both the prediction model and the measurement results showed no modulation at the specular direction. However, close to the specular direction very high modulation could be seen.

When analysing the modulation waveform in the frequency domain, it was seen that there is an initial high amplitude at a frequency three times the rotation frequency of the blades. Beyond that, further harmonics could be seen, which are due to the complex interactions between each blade and the tower.

Although there are variations in the modulation at different frequencies and polarisation, the general characteristics of the modulation waveform is constant and is primarily dependent on the observation angle.

3 TERRAIN MODELLING:

Terrain effects play an important role in the design of ground to air communication links. Accurate and reliable knowledge of these effects can help in determining the area of coverage and leads to better estimates of the signal strength at the receiver. For the work carried out in this project, it was considered necessary to incorporate these effects in the final guideline formulation.

The terrain effects may under certain circumstances be favourable for example when a hill is between the wind turbine and the receiver. Conversely when the hill is blocking the transmitter the effect is unfavourable.

This chapter describes the terrain modelling techniques adopted. The terrain model was not validated experimentally. However, comparison with other techniques and other experimental measurements which appear in previous literature is detailed.

3.1 Model development and Comparison Results

At microwave frequencies, hill obstacles can be considered to be a series of perfectly sharp knife edges and the finer details of the structure of the hills can be ignored. This is applicable to the work carried out for this project. Based on knife edges, a model was developed which predicts the attenuation caused by such obstacles.

The developed algorithm is based on the work presented by Vogler [4]. This technique is preferred because of the accuracy of the results obtained when compared with previously published experimental measurements and because of the ease of the computational implementation for any number of obstacles.

The model has been verified by comparing the predicted results with the experimental measurements made by Giovaneli [3] with differences being less than 1 dB for the two cases presented. Table 3.1 shows the results obtained by using 3 different methods when applied to the same set of data.

The theory for the developed method can be found in Appendix A.

Table 3.1 Comparison of diffraction loss using different techniques

<i>Parameters</i>	<i>Path 1</i>	<i>Path 2</i>
Frequency (MHz)	213	450
Distance a (km)	60.2	5.4
Distance b (km)	6.2	10.6
Distance c (km)	17	84
Height h1 (m)	181	228
Height h2 (m)	167.57	227.45
Loss (dB) Giovaneli [3]	24.3	37.18
Loss (dB) Deygout[2]	23.9	37.62
Loss (dB) [Developed Programme]	23.3	36.44
Measured Loss (dB) Giovaneli [3]	24	38

4 GUIDELINE FORMULATION

Given the necessary parameters, the aim of this formulation is to compute the carrier to interference (C/I) ratio at the receiver. By comparing this value with the minimum needed for proper operation of the receiver, a decision could be made on the acceptability of the wind turbine installation.

When working out the formulation, for simplicity, we shall assume a flat earth model ignoring the terrain model effects. These can be added as an extra attenuation term if required. In fact the developed software which will be provided as a deliverable will give the user the option of including up to two obstacles in any of the radio paths.

4.1 Parameter Definition

The following parameters will be used in the formulations:

P_t (dB) is the power of the transmitted signal

G_{tw} (dB) is the gain of transmitter in direction of turbine

G_{tr} (dB) is the gain of transmitter in direction of receiver

G_r (dB) is the gain of receiver in direction of transmitter

G_{rw} (dB) is the gain of receiver in direction of turbine

L_{tw} (dB) is the free space loss between transmitter and wind turbine

L_{tr} (dB) is the free space loss between transmitter and receiver

L_{wr} (dB) is the free space loss between wind turbine and receiver

$GWT(=10\log(4\pi\sigma/\lambda^2))$ (dB) is the gain of the wind turbine

σ (m²) is the wind turbine radar cross section

$\lambda(=c/f)$ (m) is the signal wavelength

f (Hz) is the frequency of the signal

c (m s⁻¹) is the speed of light

d_{tw} (m) is the distance between transmitter and wind turbine

d_{wr} (m) is the distance between wind turbine and receiver

d_{tr} (m) is the distance between transmitter and receiver

TW (dB) is the signal strength at the wind turbine originating from the transmitter

TWR (dB) is the indirect path (transmitter-wind turbine-receiver) signal strength at the receiver

TR (dB) is the direct path (transmitter-receiver) signal strength at the receiver

C/I (dB) is the carrier to interference ratio at the receiver

Free space loss L is given by:

$$L = 20\log\left(\frac{4\pi d}{\lambda}\right)$$

4.2 Theoretical formulation

The carrier to interference ratio at the receiver is formulated by calculating the direct path signal strength at the receiver less the reflected signal strength.

4.2.1 Indirect Path Signal Calculation

The signal strength at the wind turbine (TW) is given by:

$$\begin{aligned} TW &= P_t + G_{tw} - L_{tw} \\ &= P_t + G_{tw} - 20\log(4\pi d_{tw}) + 20\log(\lambda) \end{aligned}$$

Hence the multipath signal strength at the receiver is given by:

$$TWR = TW + GWT + G_{rw} - L_{tr}$$

$$TWR = P_t + G_{rw} + G_{rw} + GWT - 2 \times 20\log(4\pi) + 2 \times 20\log(\lambda) - 20\log(d_{tw}) - 20\log(d_{wr})$$

4.2.2 Direct Path Signal Calculation

The direct path signal TR is given by:

$$TR = G_r + G_{rt} - L_{tr}$$

$$TR = G_r + G_{rt} - 20\log(4\pi) - 20\log(d_{tr}) + 20\log(\lambda)$$

4.2.3 Carrier To Interference Ratio Calculation

The final part of the formulation is to calculate the carrier to interference ratio at the receiver. This is simply given by:

$$C/I = TR - TWR$$

And using the above equation for the indirect and the direct path signal strengths, C/I can be computed.

5 SOFTWARE IMPLEMENTATIONS

Software programs for the models were written in C++ under a PC environment. The software is capable of the following tasks:

- (a) Computing the attenuation due to terrain.
- (b) Computing the Radar Cross Section of the Wind Turbine.
- (c) Computing the Carrier to Interference Ratio at the Receiver.

5.1 **Terrain Model Program**

This program computes the terrain attenuation between the transmitter, wind turbine and receiver. The user is also given the option of using a flat earth model if required.

Program Name: terrain.exe

Source code names: main.cpp, terrain.cpp

Parameters required:

- (a) Frequency of signal.
- (b) Number of obstacles.
- (c) Heights of obstacles.
- (d) Distances between Obstacles.

5.2 **Radar Cross Section Program**

This program computes the maximum wind turbines radar cross section.

Program Name: rcs.exe

Source code Names: main.cpp, rcs.cpp

Parameters required:

- (a) Frequency of Signal.
- (b) Location Co-ordinates of transmitter.
- (c) Location Co-ordinates of wind turbine.
- (d) Blade co-ordinates of turbine.

5.3 **Carrier To Interference Program**

This program computes the carrier to interference ratio.

Program Name: guideline.exe

Source code Names: main.cpp, guideline.cpp

Parameters required:

- (a) Frequency of Signal.
- (b) Location of Transmitter.
- (c) Location of Receiver.
- (d) Location of Wind Turbine.
- (e) Power of Transmitter.
- (f) Gain of Transmitter in direction of turbine.
- (g) Gain of Transmitter in direction of receiver.
- (h) Gain of Receiver in direction of transmitter.

- (i) Gain of receiver in direction of turbine.
- (j) The minimum acceptable carrier to interference ratio.

6 CONCLUSIONS

Electromagnetic modelling techniques based on PO can be used for the prediction of the characteristics of wind turbines. Test measurements on a 20:1 scale model turbine performed on an antenna range agree with predicted results using developed models. Due to experimental difficulties, the model predictions could not be accurately verified in certain regions, however, these are not expected to have any significant effect on the guidelines for the installation of wind turbines near aeronautical radio systems since the regions where the model agrees with the measurements represent the worst case of interference.

Developed terrain model results show that obstacles in the radio path can have a significant effect on the signal strength at the receiver. A computer model has been written which allows these effects to be taken into consideration in the wind turbine guidelines and the results of the model predictions agree with previously published experimental measurements.

With confidence in the PO model established, guidelines have been developed. The carrier to interference ratio at the receiver is computed based on the transmitted signal power, antenna gains, frequency and locations of the radio system components. This ratio can then be compared with the minimum acceptable at the receiver.

Software has been written to enable a decision on the effects of a wind turbine to be easily made.

7 REFERENCES

- 1 Dabis, H.S., and Chignell, R.J., 'Investigation of the Interactions Between Wind Turbines and Radio Systems Aimed at Establishing Co-Siting Guidelines', ETSU W/13/00477, 1997.
- 2 Deygout, J., 'Correction Factor for Multiple Knife-Edge Diffraction', IEEE Trans. On Antenna and Propagation, vol. 39, no. 8, pp. 1256-1258, Aug. 1991.
- 3 Giovaneli, C.L., 'An Analysis of Simplified Solutions for Multiple Knife-Edge Diffraction', IEEE Trans. On Antenna and Propagation, vol. AP-32, No. 3, pp. 297-301, March 1984.
- 4 Vogler, L. E., 'An Attenuation Function for Multiple Knife-Edge Diffraction', Radio Science, vol. 17, no. 6, pp. 1541-1546, Nov-Dec. 1982.
- 5 EUROCAE, 'Minimum Performance Specification for Airborne VHF Communications Equipment in the Frequency Range 108.000-135.975 MHz', EUROCAE-ED-24, Oct. 1975. Vogler, L. E., 'An Attenuation Function for Multiple Knife-Edge Diffraction', Radio Science, vol. 17, no. 6, pp. 1541-1546, Nov-Dec 1982.
- 6 Abramowitz, M., and Stegun, I.A., 'Handbook of Mathematical Functions', Appl. Math. Ser., Vol. 55, National Bureau of Standards, Washington, D.C., 1964.

Appendix A Terrain Model Theoretical Formulation

In this we shall briefly present the theoretical background used for the terrain model discussed in the text.

Figure A1 shows the geometry associated with the multiple knife edge diffraction problem. The geometrical quantities needed to calculate the solution for N knife edges are:

- The $N+1$ separation distances between knife edges $r_1, r_2 \dots r_{N+1}$
- The heights of the knife edges $h_1, h_2 \dots h_N$
- The heights of the transmitter h_0 and the receiver h_{N+1}
- The diffraction angles $\theta_1, \theta_2 \dots \theta_N$ which can be obtained from the separations and heights.

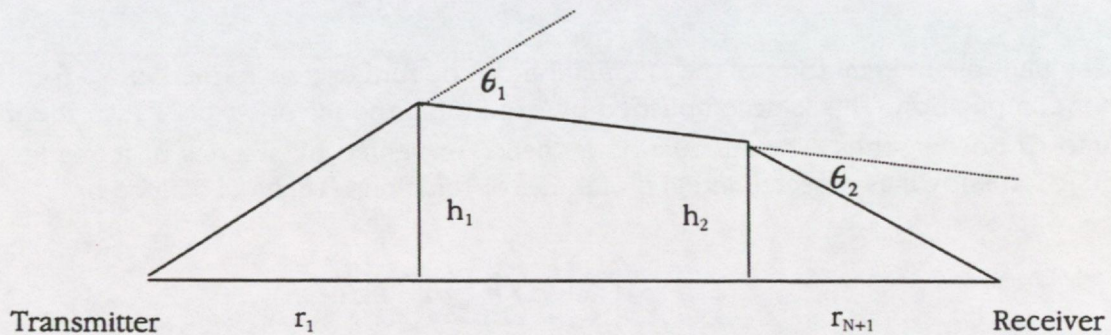


Figure A1 Geometry for Multiple Knife Edge Diffraction

The above geometric quantities together with the frequency are used to define two sets of parameters, α and β ,

$$\alpha_m = \left[\frac{r_m r_{m+2}}{(r_m + r_{m+1})(r_{m+1} + r_{m+2})} \right]^{1/2}$$

$$\beta_m = \theta_m \left[\frac{ikr_m r_{m+2}}{2(r_m + r_{m+1})} \right]^{1/2}$$

where $k = 2\pi / \lambda$ is the wave number.

With these relationships, the attenuation, A , over a path of total distance r_T and consisting of N knife-edges may be expressed as:

$$A = (1/2)^N C_N e^{\sigma_N} (1/2\pi^{1/2})^N \int_{\beta_1}^{\infty} \dots \int_{\beta_N}^{\infty} e^{2f} \cdot [\exp[-(x_1^2 + \dots + x_N^2)]] dx_1 \dots dx_N$$

where

$$f = 0 \text{ when } N = 1$$

$$f = \sum_{m=1}^{N-1} \alpha_m (x_m - \beta_m)(x_{m+1} - \beta_{m+1}) \text{ for } N \geq 2$$

$$\sigma_N = \beta_1^2 + \dots + \beta_N^2$$

$$C_N = 1 \text{ } N = 1$$

$$C_N = \left[\frac{r_2 r_3 \dots r_N r_T}{(r_1 + r_2)(r_2 + r_3) \dots (r_N + r_{N+1})} \right]$$

$$r_T = r_1 + r_2 + \dots + r_{N+1}$$

The multiple integral form of the attenuation can be further transformed into a form suitable for computation. This is accomplished by expanding the factor, $\exp(2f)$, in the integrand into its power series. The attenuation is then represented by a series of terms involving a function known as repeated integral of the error function, $I(n, \beta)$ is defined by:

$$(2/\pi^{1/2}) \int_{\beta}^{\infty} (x - \beta)^n e^{-x^2} dx = n! I(n, \beta)$$

In terms of the function $I(n, \beta)$ for which a number of computational algorithms are available, the attenuation becomes

$$A = (1/2^N) C_N e^{\sigma_N} \sum_{m=0}^{\infty} I_m$$

where

$$I_m = 2^m m! \alpha_1^m I(m, \beta_1) I(m, \beta_2) \text{ for } N = 2$$

Based on the above a program was written in C++ which computes the attenuation for any number of obstacles up to 2.

